Check for updates

JGR Biogeosciences

RESEARCH ARTICLE
10.1029/2026JG010169

Heterogeneity in Permafrost Organic Matter Molecular Composition With Depth and Ramifications Upon Thaw in the Western Siberian Lowlands

James M. Anderson[1], Martin R. Kurek[1,2], Artem G. Lim[3], Sergey V. Loiko[3], Oleg S. Pokrovsky[4], Jean-Jacques Braun[5], and Robert G. M. Spencer[1]

[1]Department of Earth, Ocean and Atmospheric Sciences and National High Magnetic Field Laboratory Geochemistry Group, Florida State University, Tallahassee, FL, USA, [2]Department of Soil and Crop Sciences, Colorado State University, Fort Collins, CO, USA, [3]BIO-GEO-CLIM Laboratory, Tomsk State University, Tomsk, Russia, [4]Geoscience and Environment Toulouse (GET), UMR 5563 CNRS University of Toulouse, Toulouse, France, [5]Centre de Pédologie Biologique, CNRS, Vandœuvre-lès-Nancy, France

Key Points:

- Permafrost peatlands of the Western Siberian Lowlands store potentially biolabile, nitrogen-enriched aliphatic dissolved organic matter within permafrost peat
- The highest proportions of nitrogenous aliphatic compounds coincide with localized "zones of DOC enrichment" within permafrost peat
- These zones of enrichment may drive non-linear biogeochemical and climate impacts from this region with ongoing permafrost thaw

Supporting Information:

Supporting Information may be found in the online version of this article.

Correspondence to:

J. M. Anderson,
janderson13@fsu.edu

Citation:

Anderson, J. M., Kurek, M. R., Lim, A. G., Loiko, S. V., Pokrovsky, O. S., Braun, J.-J., & Spencer, R. G. M. (2026). Heterogeneity in permafrost organic matter molecular composition with depth and ramifications upon thaw in the Western Siberian Lowlands. *Journal of Geophysical Research: Biogeosciences*, *131*, e2026JG010169. https://doi.org/10.1029/2026JG010169

Received 15 JUN 2026
Accepted 4 SEP 2026

© 2026 American Geophysical Union. All rights reserved, including rights for text and data mining and training of artificial intelligence technologies or similar technologies.

Abstract Northern circumpolar permafrost represents a globally significant soil organic carbon (C) reservoir. The reintroduction of this previously frozen C into the contemporary C cycle with accelerated northern climate change has raised concerns over a potential permafrost C warming feedback. Additionally, the chemically distinct molecular composition of permafrost organic C has previously been linked to its high biolability upon thaw. Despite this, few studies to date have characterized trends in the molecular composition and hence potential reactivity of this frozen C with depth in permafrost, limiting understanding of potential feedback evolution with forecast 21st century thaw trajectories. Here, we examine depth-dependent trends in dissolved organic matter (DOM) molecular composition within frozen peat cores collected from the Western Siberian Lowlands (WSL), the largest permafrost peatland system in the world. We observe a strong positive correlation between dissolved organic C (DOC) concentration and high-energy aliphatic compound relative abundance within WSL permafrost peat ($\rho = 0.81$, $p < 0.01$), with distinct "zones of enrichment" containing between 1.5-4x higher DOC concentrations and ~10 percentage point higher aliphatic DOM contribution versus surrounding permafrost peat horizons found to be present within core depth profiles. These observations, coupled with previous regional findings documenting nutrient and trace element enrichment within these depth ranges, suggest that these localized zones of enrichment may act as biogeochemical hotspots within the depth profile of WSL permafrost peat. As such, solute mobilization from these zones may drive non-linear trajectories (specifically hot moments) of regional and global thaw impacts from WSL permafrost peatlands with continued warming.

Plain Language Summary Ongoing and future thaw of permafrost soils threatens to release substantial quantities of organic carbon (C) into modern terrestrial and aquatic systems, potentially leading to enhanced greenhouse gas emissions from the permafrost domain, which has raised concerns over a permafrost C warming feedback. While previous studies have shown that the molecular composition of permafrost organic C renders it highly susceptible to microbial degradation upon thaw, relatively little work has been done up to this point characterizing trends in the composition of this organic C with depth in these perennially frozen soils. This study seeks to fill this knowledge gap by documenting depth-dependent patterns of dissolved organic matter (DOM) composition within permafrost peat of the Western Siberian Lowlands (WSL), a globally significant permafrost peatland system. We observed a strong positive relationship between dissolved organic carbon (DOC) concentration and aliphatic compound relative abundance with depth in our peat cores. Additionally, we document the presence of localized zones of DOC enrichment within core depth profiles, found to contain the largest proportion of potentially biodegradable DOM within permafrost peat. This observation suggests that these particular depth ranges may exert the strongest effects on regional ecosystem processes and global climate warming upon thaw.

1. Introduction

Since the early 1980s, the Arctic has experienced rates of warming up to four times higher than the global average, with this observed divergence largely being driven by regional ice-albedo feedbacks and ongoing changes to global energy transport processes (Rantanen et al., 2022). Among the implications of a rapidly warming northern

21698961, 2026, 9, Downloaded from https://agupubs.onlinelibrary.wiley.com/doi/10.1029/2026JG010169 by Florida State University, Wiley Online Library on [02/11/2026]. See the Terms and Conditions (https://onlinelibrary.wiley.com/terms-and-conditions) on Wiley Online Library for rules of use; OA articles are governed by the applicable Creative Commons License

climate is the potential for widespread thaw of permafrost soils, which may alter regional hydrologic and biogeochemical regimes through the deepening of groundwater flowpaths, the release of heavy metal and nutrient elements, and the remobilization of vast quantities of frozen organic matter (OM) long removed from the global carbon (C) cycle (Lim et al., 2021; Turetsky et al., 2020; Walvoord & Striegl, 2007). It has previously been estimated that northern circumpolar permafrost may store up to 1,466 Pg of perennially frozen C (Tarnocai et al., 2009), with a significant portion of this sizable cryopreserved C reservoir found to be composed of low molecular weight, highly saturated aliphatic compounds that are rapidly consumed by microbial communities upon thaw (Drake et al., 2015; Spencer et al., 2015). Taken together, the immense size and high biodegradability of the permafrost C reservoir renders this thawing C stock capable of enhancing northern greenhouse gas (GHG) emissions with continued warming and wetting of the permafrost domain, raising concerns over a potential permafrost C warming feedback (PCF) with projected 21st century Representative Concentration Pathway (RCP) and permafrost degradation trajectories (Miner et al., 2022; Turetsky et al., 2020).

Past research centered on understanding the biogeochemical and climatic repercussions of thawing permafrost has largely focused on quantifying regional variability in OM stocks across the permafrost domain, characterizing the molecular nature of these frozen OM stocks using advanced analytical techniques, and determining the reactivity of this aged and ancient OM upon its remobilization into modern terrestrial and aquatic systems (Cheng et al., 2022; Drake et al., 2015; MacDonald et al., 2021; Olefeldt et al., 2016; Strauss et al., 2013; Tarnocai et al., 2009; Wild et al., 2022). While these efforts have provided tremendous insight into the nature of the permafrost C pool, understanding of how OM stock sizes, molecular composition, and in turn reactivity upon thaw co-vary with depth in permafrost deposits remains limited. This paucity therefore constrains the accuracy of permafrost-focused earth system models that omit crucial depth-resolved C stock, composition, and reactivity data, and in turn limits current ability to predict future PCF magnitude under potential 21st century thaw scenarios.

Prior work assessing depth-dependent patterns of OM composition and biodegradability focused on ice-rich yedoma permafrost has highlighted higher relative abundance of highly saturated aliphatic compounds, low molecular weight organic acids (LMWOAs), and corresponding higher percent biodegradable DOC with increasing depth and deposit age, thus indicating the greater apparent biolability of OM stored within deeper, older permafrost deposits (Ewing et al., 2015; Heslop et al., 2019; Stapel et al., 2018). Significantly, these studies also note higher proportions of this deep permafrost OM potentially remineralized as CH_4 upon thaw when compared to OM pools of shallower, younger yedoma deposits, as determined by biodegradation experiments mimicking anoxic thaw slump environments (Heslop et al., 2019). While these observations from the yedoma domain therefore represent one potential PCF trajectory, namely greater permafrost climate warming potential with increasing depth of thaw, studies from the Western Canadian Arctic demonstrate that the legacy of past landscape change plays a key role in shaping depth-dependent patterns of geochemical composition within permafrost sediment profiles (Lacelle et al., 2019). Specifically, within frozen glaciogenic sediments of the Peel Plateau region, significant heterogeneity has been observed in patterns of OM composition and solute concentration with depth owing to the presence of localized paleo active layers formed during early Holocene climate fluctuations (Lacelle et al., 2019). This observation therefore adds an additional layer of complexity to the relatively uniform patterns observed in undisturbed yedoma depth profiles, as well as demonstrates the importance of local and regional-scale variability in shaping impacts of future thaw.

When examining how local and regional patterns of OM composition and reactivity with depth in northern permafrost may dictate future PCF magnitude, one particularly significant component of the permafrost domain requiring consideration is the extensive permafrost peatland system of the Western Siberian Lowlands (WSL). In Western Siberia, permafrost and permafrost-free peatlands cover 592,000 km^2, exceeding more than 50% of all regional area in the taiga zone (Pastukhov et al., 2021), with the WSL specifically representing the largest permafrost peatland system in the world (Serikova et al., 2019). Air temperatures in this region have been rising faster than the Arctic as a whole (Frey & Smith, 2005; Serreze et al., 2002), threatening northward migration of the WSL permafrost boundary over the course of the current century (Raudina et al., 2018). Previous studies have estimated that this immense network of frozen bogs may store between 10 and 100 kg C m^{-2} (Hugelius et al., 2020), indicating a sizable frozen C stock of which large portions may be vulnerable to decomposition following permafrost degradation, particularly via remobilization into expanding thermokarst lake and pond systems as dissolved organic matter (DOM). Across the Siberian permafrost domain, climate warming and wetting trends over recent decades have contributed to net lake area increases of 0.89% for the 1999–2013 period

21698961, 2026, 9, Downloaded from https://agupubs.onlinelibrary.wiley.com/doi/10.1029/2026JG010169 by Florida State University, Wiley Online Library on [02/11/2026]. See the Terms and Conditions (https://onlinelibrary.wiley.com/terms-and-conditions) on Wiley Online Library for rules of use; OA articles are governed by the applicable Creative Commons License

and 4.15% for the 1999–2018 period (Pastukhov et al., 2021), as well as increases in epilimnetic water temperature, alkalinity, and calculated pCO_2, over time (Drake et al., 2018). Observations from across Alaska have previously demonstrated the potential of deep, biolabile permafrost C pools to fuel thermokarst lake CH_4 emissions, particularly in regions characterized by ice-rich permafrost deposits (Walter Anthony et al., 2016). Given the susceptibility of WSL permafrost peat to abrupt thaw owing to its high porosity and large syngenetic ice content (Kuzmina et al., 2023; Pastukhov et al., 2021), coupled with the potential of these poorly drained lowlands to act as a substantial global CH_4 source with ongoing changes to regional climate, these observations directly implicate WSL permafrost peatlands and their substantial frozen C stocks in the discussion of a PCF. Moreover, the susceptibility of these peatlands to thermokarst processes that expose deep, potentially biolabile frozen C pools to decomposition emphasizes the need to understand depth-dependent trends in OM composition and reactivity within perennially frozen WSL peat, allowing for more accurate predictions to be made as to the future climate forcing potential of these systems.

The current body of literature dedicated to characterizing the geochemical composition of WSL permafrost peat has documented considerably higher (∼3x) DOC and inorganic solute concentrations within perennially frozen peat when compared to seasonally unfrozen active layer porewaters (Lim et al., 2021). Additionally, optical and size exclusion-based methods have previously highlighted the strong potential of permafrost peat OM in these systems to contribute to regional GHG emissions, as indicated by its low molecular weight, highly aliphatic molecular composition (Kurashev et al., 2024; Lim et al., 2022), thus implying the potentially high biolability of this OM upon thaw (Spencer et al., 2015). A particularly noteworthy feature consistently documented by studies from this region is the presence of localized zones of DOC and inorganic solute enrichment within permafrost peat, commonly observed to occur approximately 30–50 cm below the active layer of these peatlands (Lim et al., 2021). These "zones of solute enrichment" within permafrost peat are specifically characterized by markedly higher DOC, Fe, P, Mg, Ca, Mn, and Sr concentrations than surrounding permafrost layers (Lim et al., 2021), thereby suggesting that these depth ranges may play a particularly significant role in shaping future biogeochemical and climate impacts of WSL permafrost peatland degradation with sustained regional warming.

In this study, we build upon this body of knowledge by examining patterns of DOM molecular composition with depth across several thaw-vulnerable WSL permafrost peat profiles using ultrahigh-resolution Fourier Transform-Ion Cyclotron Resonance mass spectrometry (FT-ICR MS). FT-ICR MS has previously been employed in the characterization of DOM across a wide range of complex environmental mixtures owing to its unparalleled mass resolving power, thus providing the highest resolution insight into DOM molecular composition in aquatic systems (Heslop et al., 2019; Kurek et al., 2025; Smith et al., 2018), with this molecular composition inextricably linked to reactivity (i.e., biolability, photolability) (Kurek et al., 2025; Starr et al., 2024). Coupled with previous observations made describing the presence of localized zones of solute enrichment within permafrost peat of this region (Kuzmina et al., 2023; Lim et al., 2021; Raudina & Loiko, 2019), we assess how variability in DOM molecular composition and bulk solute remobilization potential with depth may collectively shape regional biogeochemical impacts as well as global PCF strength under future thaw scenarios.

2. Materials and Methods

2.1. Study Site Description

Sample sites are located within the discontinuous permafrost zone of the southern tundra (Tazovsky) biome (N67.3°, E78.7°) of the WSL, part of the Tazovsky District (Yamalo-Nenets Autonomous Okrug) (Figure 1a) on the northern portion of the Pur-Taz interfluve. Regional climate ranges from moderately humid and cold in summer to cold and snow-deficient in winter, with a mean annual air temperature of ∼−9.1°C and annual precipitation of 360 mm (Raudina & Loiko, 2019). This region is located within the watershed of the Taz River, which drains predominantly Pleistocene sand and loess-like silts (Lim et al., 2021). The Tazovsky landscape is characterized by extensive polygonal permafrost peat plateaus with an abundance of positive relief (polygons) and negative relief (hollows and frost cracks) micro-landscapes (Raudina & Loiko, 2019) (Figures 1b and 1c), as well as thermokarst landforms such as lakes and drained lake basins (Figure 1b). Peat in this region has been actively forming since the early Holocene, with the onset of colder climate conditions between 9 and 4.5 thousand years ago leading to freezing and slower contemporary peat accumulation rates (Pastukhov et al., 2021). Average peat depth for frozen polygonal bogs ranges from 2.0 to 4.0 m, with a mean annual active layer thickness of ∼41 cm (Raudina & Loiko, 2019). Vegetation community composition is largely oligotrophic, indicating predominantly ombrotrophic

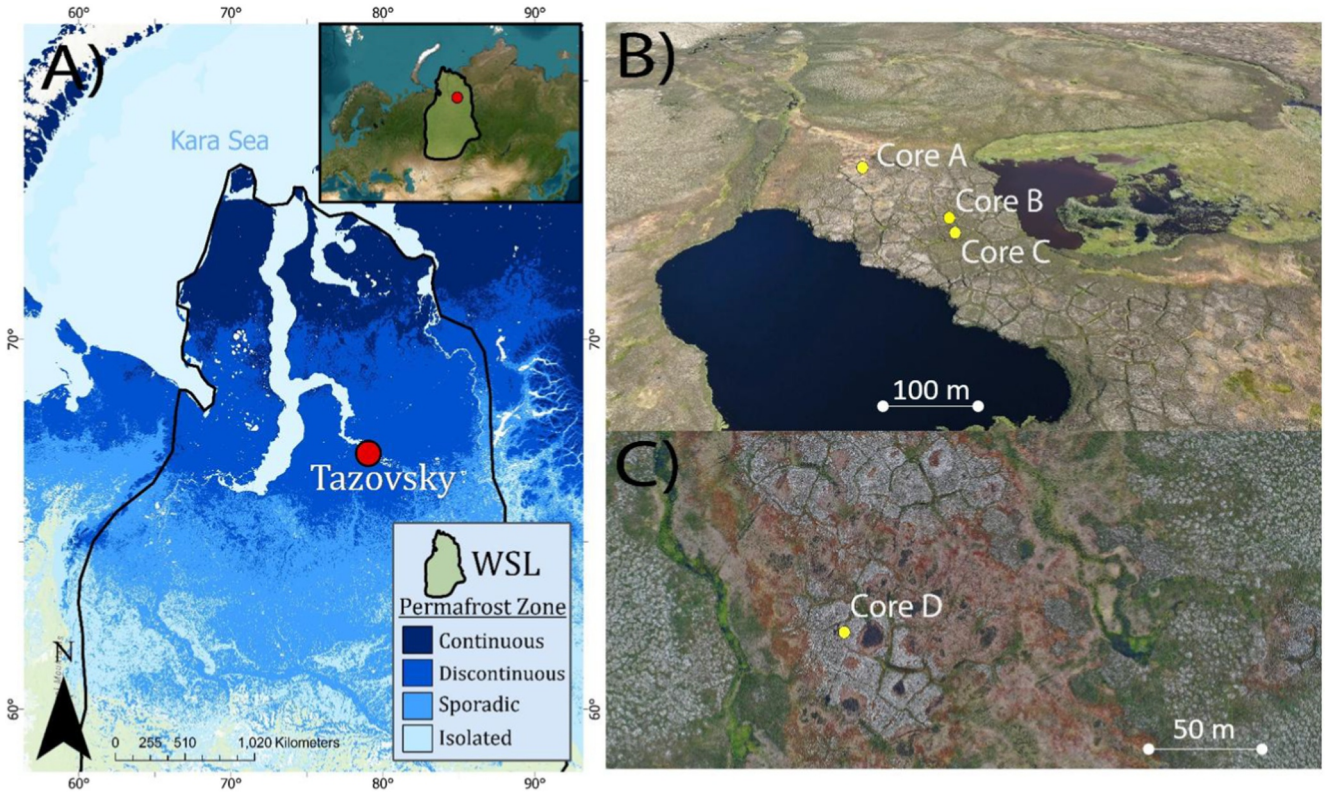


Figure 1. Panel (a) shows the Tazovsky site within the Western Siberian Lowlands. Panel (b) shows A, B and C core sampling locations within the Tazovsky site along a polygonal permafrost peat plateau between a thermokarst lake and a drained thermokarst lake basin (aerial view). Panel (c) shows Core D sampling location also within the Tazovsky site on the flat polygon of a polygonal permafrost peat plateau.

conditions (Raudina & Loiko, 2019). Soil classifications for polygons and hollows are Hyperorganic Hemic Epicryic Histosols and Epifibric Endohemic Cryic Histosols, respectively (Kuzmina et al., 2023; Pastukhov et al., 2021; Raudina & Loiko, 2019). On polygons, the upper 50 cm of peat deposits consists mainly of residues of dwarf shrubs, hypnum mosses, grasses, lichens, sphagnum mosses (*Sphagnum fuscum, S. majus*) and, less commonly, wood (Pastukhov et al., 2021). In the hollows, the upper 50 cm of peat deposits consist mainly of sphagnum mosses, cotton grass, sedges, and less commonly, grasses (Raudina & Loiko, 2019).

2.2. Peat Core and Porewater Sampling

Four intact peat cores (Core A: N67.358138°, E78.709593°; Core B: N67.357520°, E78.706847°; Core C: N67.357491°, E78.7061626°; Core D: N67.379508°, E78.696448°) were collected from the Tazovsky site, with one representative core collected from each microsite along the thaw sequence (Core D: bog, Core C: trough, Core B: transitional fen, and Core A: peat–mineral fen). This design was chosen to resolve depth-dependent contrasts between active layer porewaters and underlying pore ice (hereafter broadly referred to as permafrost peat) across the landscape gradient. Although no within-site replicates were collected, the representativeness of this study design is supported by previous multi-core studies at Tazovsky, which showed limited within-unit variability in soluble organic carbon and consistent vertical patterns in physical and hydrochemical properties among comparable microtopographic settings (Kuzmina et al., 2023; Loiko et al., 2019).

In all cores, the active layer was entirely developed within the peat. At the time of sampling, the active layer thickness was 35 ± 5 cm for Core A, 55 ± 5 cm for Core B, 35 ± 5 cm for Core C, and 23 ± 5 cm for Core D. Cores (4 cm diameter) were retrieved using a Russian peat corer following established procedures for the study area (Kuzmina et al., 2023; Lim et al., 2021, 2022). Each core was sectioned with a ceramic blade into 5-cm intervals, and into 10-cm intervals below 100 cm depth, with permafrost sections of cores thawed at room temperature (under oxic conditions) over a period of several hours. Porewaters collected from the active layer and permafrost core sections were first extracted through a pre-cleaned 100-μm nylon mesh under local confining

21698961, 2026, 9, Downloaded from https://agupubs.onlinelibrary.wiley.com/doi/10.1029/2026JG010169 by Florida State University, Wiley Online Library on [02/11/2026]. See the Terms and Conditions (https://onlinelibrary.wiley.com/terms-and-conditions) on Wiley Online Library for rules of use; OA articles are governed by the applicable Creative Commons License

21698961, 2026, 9, Downloaded from https://agupubs.onlinelibrary.wiley.com/doi/10.1029/2026JG010169 by Florida State University, Wiley Online Library on [02/11/2026]. See the Terms and Conditions (https://onlinelibrary.wiley.com/terms-and-conditions) on Wiley Online Library for rules of use; OA articles are governed by the applicable Creative Commons License

pressure (1–5 kg cm^{-2}, depending on sample moisture). The resulting slurry was centrifuged for 15 min at 1,096 g, and the supernatant was filtered through 0.45 μm filters; the first 10 mL of filtrate was discarded.

2.3. Sample Preparation and Analysis

2.3.1. Dissolved Organic Carbon (DOC) and Total Nitrogen (TN)

Filtered peat water samples were acidified using HCl and analyzed for DOC and Total Nitrogen (TN) concentrations using a Shimadzu TOC-L CPH high-temperature catalytic oxidation total organic carbon analyzer with an added TN unit (Shimadzu Corp., Kyoto, Japan). Samples were sparged according to established methodology (Textor et al., 2018), and final DOC concentrations were determined using nondispersive infrared radiation (NDIR) detection. TN was measured for Cores A, B, and C (measurements were not available for Core D given that it was collected as part of a separate sampling campaign) while DOC concentrations were measured for all cores.

2.3.2. Solid-Phase Extraction

Sample DOM was isolated using solid-phase extraction (SPE) to a target concentration of 40 μg C mL^{-1} assuming a 65% recovery rate (Dittmar et al., 2008). Samples were first diluted to a working DOC concentration for SPE using ultrapure Milli-Q water and acidified to pH 2 using HCl. 100 mg Bond-Elut PPL cartridges were given an initial rinse and left to soak overnight with high performance liquid chromatography (HPLC) grade methanol. The following morning, cartridges were drained and rinsed with ultrapure Milli-Q water and methanol and conditioned with pH 2 Milli-Q water. Samples were then passed through conditioned cartridges, rinsed with pH 2 ultrapure Milli-Q water, and dried with a flow of inert gas (ultrapure N_2). Extracted sample DOM was eluted from dry cartridges with 1 mL HPLC grade methanol into precombusted (550°C, >4 hr) 1.5-mL amber LC vials, yielding the final operationally extracted peat porewater DOM pool to be used for analysis.

2.3.3. FT-ICR MS

Samples were analyzed on a custom-built FT-ICR MS equipped with a passively shielded 9.4-T magnet (Oxford Instruments, Abingdon, Oxfordshire, UK) and horizontal 220 mm bore diameter at the National High Magnetic Field Laboratory (Tallahassee, FL, USA; Stenson et al., 2003; Kaiser et al., 2011). Analysis was conducted in negative electrospray ionization (ESI-) mode, with direct infusion of negatively charged ions at a constant flow rate of 3 μL min^{-1}. Spray needle voltage was held at −2,500 V throughout the experiment, with mass spectra collected as the sum of 100 co-added scans for each sample. Sample spectra were internally calibrated from a highly abundant oxygen-containing alkylation series with a "walking calibration" equation ($141 < m/z < 1{,}000$) (Kurek et al., 2020; Savory et al., 2011). Mass spectral peaks with a six times greater signal magnitude than the baseline root-mean-square (RMS) noise level were ultimately selected for export to a final peak list. Elemental composition assignments were made using PetroOrg© within the molecular bounds of $C_{1–45}H_{1–92}N_{0–4}O_{1–25}S_{0–2}$ (error ± 0.3 ppm) (Kellerman et al., 2019; Slentz et al., 2025).

2.3.4. Data Processing and Analysis

Data processing following elemental composition assignment was performed using Microsoft Excel and *R* Statistical Computing software (version 4.4.3) (R Core Team, 2021). Molecular characteristics of individual formulae were classified based on calculated elemental ratios (i.e., H/C, O/C, N/C, S/C), Modified Aromaticity Index (AI_{mod}) (Koch & Dittmar, 2006), as well as Nominal Oxidation State of C (NOSC) (Boye et al., 2017). Based on elemental composition, sample molecular formulae were grouped by heteroatom class (CHO, CHON, CHOS, CHONS, hereafter referred to as formula group) providing an indication of DOM relative heteroatom-enrichment (Kurek et al., 2020). From calculated molecular properties, formulae were grouped into representative natural DOM compound classes using the following molecular parameters: condensed aromatic compounds ($AI_{mod} > 0.67$), polyphenolic compounds ($0.67 \geq AI_{mod} \geq 0.5$), highly unsaturated compounds ($AI_{mod} < 0.5$ and $H/C < 1.5$, with highly unsaturated-high O/C compounds classified by $O/C \geq 0.5$ and highly unsaturated-low O/C compounds by $O/C < 0.5$), and finally aliphatic compounds ($H/C \geq 1.5$) (derived from Kellerman et al., 2019; Šantl-Temkiv et al., 2013). DOM molecular characteristics were calculated using relative abundance-weighted averages of constituent sample formula molecular properties described above, with statistical significance ($p < 0.05$) assessed via Welch's *t*-test when data followed a normal distribution (Shapiro-Wilk test, $p \geq 0.05$) or

21698961, 2026, 9, Downloaded from https://agupubs.onlinelibrary.wiley.com/doi/10.1029/2026JG010169 by Florida State University, Wiley Online Library on [02/11/2026]. See the Terms and Conditions (https://onlinelibrary.wiley.com/terms-and-conditions) on Wiley Online Library for rules of use; OA articles are governed by the applicable Creative Commons License

the Mann-Whitney U Test (Mann & Whitney, 1947) when sample data was not normally distributed (Shapiro-Wilk test, $p < 0.05$) (Shapiro & Wilk, 1965). Principal Component Analysis (PCA) was conducted using FactoMineR and factoextra packages in *R*, with variables first scaled to unit variance via z-score standardization to ensure comparability (Lê et al., 2008; Slentz et al., 2025). Spearman's rank correlations were computed using the cor.test base *R* function, and the ggplot2 package was used for figure generation (Lê et al., 2008; Wickham, 2016).

3. Results

3.1. Depth-Dependent Trends in DOC and TN

Porewater DOC concentrations varied considerably with depth across the four cores, with observed values ranging from 139 to 1,181 mg/L, 208–1,113 mg/L, 125–573 mg/L, and 65–1,896 mg/L for Cores A, B, C, and D, respectively (Figure 2; Table 1). In agreement with previous studies from this region (Kuzmina et al., 2023; Lim et al., 2021), elevated DOC concentrations were observed in samples collected from permafrost sections of cores (614.9 ± 390 mg/L) ($n = 59$) when compared to porewaters of the seasonally unfrozen active layer (221.5 ± 109) ($n = 17$) ($p < 0.01$) (Figure 2; Table 1; Table S1). Notably, significant heterogeneity was observed in DOC concentrations within permafrost sections of cores, with localized "zones of DOC enrichment" found to be present within certain depth ranges as previously documented by several studies (Figure 2) (Kuzmina et al., 2023; Lim et al., 2021). These zones of DOC enrichment were identified as discrete depth intervals within permafrost peat exhibiting DOC concentrations ~1.5-4x higher than the mean DOC concentration of adjacent overlying and underlying permafrost horizons outside the enriched interval. These zones were identified where elevated DOC values persisted across at least two consecutive sampling depths, forming a localized DOC maximum distinct from surrounding permafrost layers, with Core D exhibiting the most pronounced maximum and Core B containing potentially two distinct zones of DOC enrichment between 60 and 120 cm (despite these zones being less pronounced in comparison to other cores) (Figure 2; Table 1). Specifically, mean DOC concentrations were measured as 964.9 ± 395 mg/L within these zones of enrichment ($n = 22$) compared to 406.8 ± 187 for surrounding permafrost horizons ($n = 37$), with this difference found to be statistically significant ($p < 0.01$). Measured TN concentrations closely mirrored DOC trends with depth for Cores A, B, and C ($\rho = 0.74$, $p < 0.01$) exhibiting local peaks corresponding with these zones of DOC enrichment within permafrost peat (Table 1).

3.2. FT-ICR MS: DOM Molecular Characteristics

3.2.1. DOM Molecular Composition With Depth

Clear downcore trends in DOM composition were observed via FT-ICR MS, revealing key distinctions in the molecular speciation of DOM pools between different depth ranges of collected peat cores. Thaw state of peat (permafrost vs. seasonally thawed) exhibited strong control over DOM molecular composition, with generally higher H/C ratios and hence more highly saturated DOM identified within permafrost peat (1.20 ± 0.07) when compared to active layer porewaters (1.03 ± 0.07) ($p < 0.01$) (Figure 3a; Table 1; Table S1). In addition to being more saturated, permafrost peat DOM was relatively enriched in nitrogen (N), as indicated by higher sample N/C ratios (0.037 ± 0.01) versus active layer DOM (0.012 ± 0.003) ($p < 0.01$) (Figure 3b; Table 1). Sample DOM O/C ratios did not vary considerably between permafrost peat and active layer porewaters, and near-zero S/C ratios and CHOS relative abundance were observed within both active layer and permafrost samples (Table 1). The relative abundance of CHON-containing formulae within permafrost peat (24.19 ± 8.63) was found to be considerably higher than in active layer porewaters (8.42 ± 3.96) ($p < 0.01$), with the latter shown to be comparatively dominated by CHO-containing molecular formulae driven by this relative permafrost organic N enrichment (Figure 4; Table 1). Calculated AI_{mod} and NOSC values for samples revealed similar trends, with generally lower values observed for permafrost peat DOM when compared to DOM of active layer porewaters, indicating a less aromatic, highly reduced DOM pool within perennially frozen versus active layer peat of this region (Figures 3c and 3d; Table 1).

Downcore trends in DOM H/C, N/C, and CHON relative abundance closely mirrored observed trends in DOC concentration with depth ($\rho = 0.78$, $p < 0.01$ for H/C; $\rho = 0.70$, $p < 0.01$ for N/C; $\rho = 0.69$, $p < 0.01$ for CHON within pooled samples). These relationships were found to be much stronger for samples located within permafrost sections of cores ($\rho = 0.74$, $p = 0$ for H/C; $\rho = 0.62$, $p < 0.01$ for N/C; $\rho = 0.66$, $p < 0.01$ for CHON), versus samples from the seasonally unfrozen active layer ($\rho = 0.33$, $p = 0.18$ for H/C; $\rho = -0.42$, $p = 0.1$ for N/C; $\rho = -0.5$, $p = 0.04$ for CHON). Specifically, the observed localized zones of DOC enrichment within permafrost

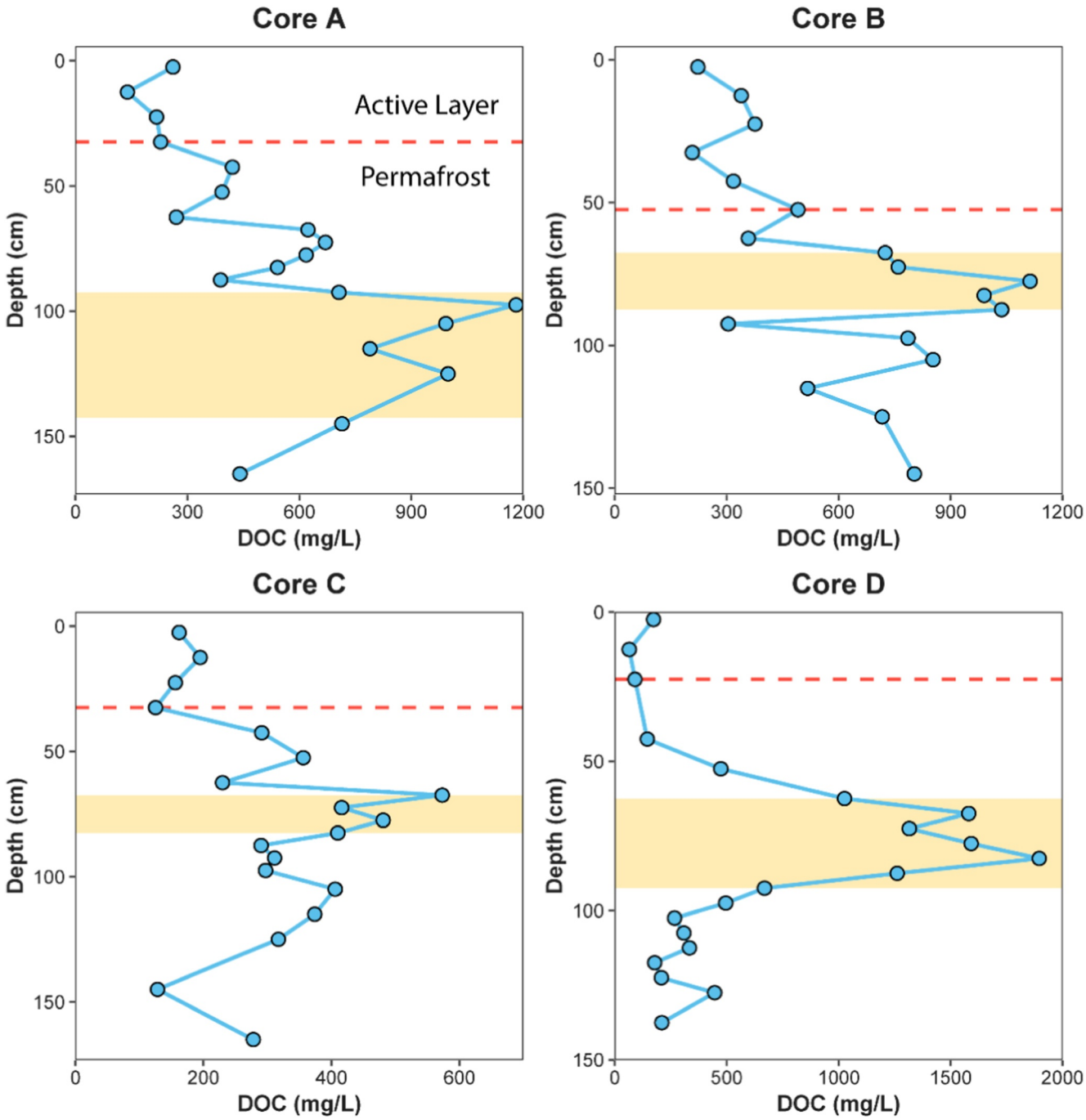


Figure 2. Trends in DOC concentration with depth for peat cores where red dashed lines indicate maximum annual active layer depth and shaded yellow regions indicate observed zones of DOC enrichment within permafrost peat.

peat of these cores (~70–90 cm depth for Cores B, C, and D and ~90–150 cm depth for Core A) (Figure 2) appeared to coincide with the highest sample DOM H/C and N/C values, as well as the highest local relative abundances of CHON-containing formulae within permafrost (Figures 3a, 3b and 4). When considered separately from surrounding permafrost layers, samples from zone of enrichment depth ranges were found to contain considerably higher H/C (1.27 ± 0.04), N/C (0.04 ± 0.01), and CHON relative abundance (31.10 ± 6.36) values than adjacent permafrost samples within core depth profiles marked by lower DOC concentrations ($p < 0.01$) (Figures 3a, 3b, and 4; Table 1). These observations were further supported by observed trends in AI_{mod} and

21698961, 2026, 9, Downloaded from https://agupubs.onlinelibrary.wiley.com/doi/10.1029/2026JG010169 by Florida State University, Wiley Online Library on [02/11/2026]. See the Terms and Conditions (https://onlinelibrary.wiley.com/terms-and-conditions) on Wiley Online Library for rules of use; OA articles are governed by the applicable Creative Commons License

Journal of Geophysical Research: Biogeosciences 10.1029/2026JG010169

Table 1

*Averages ± Standard Deviations of DOC and Total Nitrogen Concentrations, Formula-Averaged (Weighted) and % Abundance Values for Peat Core Depth Regions Where AL = Active Layer, P = Permafrost, *P = Zone of Enrichment Within Permafrost, CA = Condensed Aromatics, Pph = Polyphenolics, HU-LO = Highly Unsaturated–Low O/C, HU-HO = Highly Unsaturated–High O/C, Ali = Aliphatics*

Core	Type	DOC (mg/L)	TN (mg/L)	Mass	H/C	O/C	N/C	S/C	CHO%	CHON%	CHOS%	CHONS%	AI_{mod}	NOSC	CA%	Pph %	HU-LO%	HU-HO%	Ali%
A	AL	211 ± 52	3 ± 1	577.5 ± 20.2	1.03 ± 0.02	0.51 ± 0.01	0.01 ± 0	/	93.34 ± 0.98	5.66 ± 0.47	1 ± 0.59	/	0.36 ± 0.01	0.02 ± 0.03	2.39 ± 0.4	20.18 ± 2.35	27.83 ± 1.99	46.31 ± 1.35	3.29 ± 0.69
A	P	485 ± 134	23 ± 17	545.5 ± 22.9	1.15 ± 0.03	0.51 ± 0.02	0.02 ± 0.01	/	89.3 ± 5.95	10.34 ± 5.81	0.37 ± 0.45	/	0.29 ± 0.02	−0.07 ± 0.03	1.03 ± 0.35	14.43 ± 2.35	28.77 ± 3.6	43.78 ± 5.34	11.99 ± 3.11
A	*P	897 ± 191	80 ± 18	526.7 ± 10.1	1.25 ± 0.03	0.49 ± 0.01	0.05 ± 0.01	/	59.01 ± 8.46	37.75 ± 7.91	3.19 ± 1.76	0.05 ± 0.09	0.25 ± 0.01	−0.12 ± 0.05	0.75 ± 0.29	9.4 ± 1.62	32.9 ± 2.38	32.35 ± 1.58	24.6 ± 3.99
B	AL	326 ± 104	9 ± 7	585.1 ± 20.7	1.04 ± 0.03	0.53 ± 0.01	0.01 ± 0.01	/	93.47 ± 3.34	6.14 ± 3.55	0.4 ± 0.38	/	0.35 ± 0.02	0.04 ± 0.07	2.29 ± 0.86	21.09 ± 2.81	24.78 ± 4.93	48.38 ± 2.78	3.46 ± 1.06
B	P	620 ± 225	75 ± 32	494.8 ± 29.1	1.22 ± 0.07	0.5 ± 0.01	0.04 ± 0.01	/	74.43 ± 4.13	25.22 ± 4.02	0.35 ± 0.25	/	0.26 ± 0.04	−0.11 ± 0.08	0.84 ± 0.86	10.14 ± 4.89	31.49 ± 3.99	36.48 ± 5.06	21.04 ± 6.64
B	*P	925 ± 173	93 ± 29	500.8 ± 21	1.26 ± 0.05	0.51 ± 0.01	0.05 ± 0	/	67.44 ± 6.22	31.2 ± 4.37	1.36 ± 1.91	/	0.24 ± 0.03	−0.1 ± 0.05	0.56 ± 0.37	8.54 ± 3.23	29.15 ± 3.12	37.45 ± 3.03	24.3 ± 5.73
C	AL	160 ± 29	22 ± 27	565.9 ± 32.5	1 ± 0.07	0.52 ± 0.01	0.02 ± 0	/	87.15 ± 1.8	12.12 ± 1.63	0.73 ± 0.22	/	0.39 ± 0.05	0.09 ± 0.06	5.12 ± 3.83	23.41 ± 9.65	26.84 ± 5	41.54 ± 7.7	3.09 ± 1.33
C	P	298 ± 74	47 ± 16	509.1 ± 16	1.17 ± 0.07	0.49 ± 0.01	0.03 ± 0.01	/	77.45 ± 3.71	21.56 ± 3.62	0.99 ± 0.35	/	0.29 ± 0.04	−0.09 ± 0.06	1.05 ± 1.52	12.73 ± 5.27	34.69 ± 3.58	38.08 ± 3.01	13.45 ± 4.18
C	*P	470 ± 76	77 ± 7	491.8 ± 17.3	1.26 ± 0.01	0.49 ± 0.01	0.04 ± 0	/	73.47 ± 0.26	25.51 ± 0.19	1.03 ± 0.4	/	0.24 ± 0	−0.15 ± 0.02	0.38 ± 0.11	7.56 ± 0.5	34.45 ± 1.18	36.57 ± 1.05	21.04 ± 1.31
D	AL	109 ± 57	NA	605.6 ± 28.4	1.03 ± 0.14	0.52 ± 0.02	0.01 ± 0	/	86.73 ± 2.27	11.71 ± 3.89	1.56 ± 1.72	/	0.37 ± 0.09	0.06 ± 0.12	5.42 ± 3.31	24.87 ± 12.3	25.19 ± 5.32	38.65 ± 3.66	5.88 ± 6.93
D	P	307 ± 128	NA	534.1 ± 26.2	1.14 ± 0.05	0.5 ± 0.01	0.04 ± 0	/	74.72 ± 3.84	23.64 ± 3.49	1.62 ± 0.53	0.02 ± 0.06	0.3 ± 0.03	−0.02 ± 0.05	1.43 ± 1.25	16.2 ± 4.3	30.98 ± 4.01	39.92 ± 4.52	11.48 ± 3.42
D	*P	1,335 ± 405	NA	499.4 ± 19.8	1.29 ± 0.05	0.52 ± 0.03	0.04 ± 0	/	69.5 ± 1.88	28.52 ± 1.97	1.97 ± 1.62	/	0.22 ± 0.02	−0.14 ± 0.09	0.42 ± 0.23	7.04 ± 2.34	28.52 ± 7.26	36.84 ± 11.27	27.19 ± 7.9

21698961, 2026, 9, Downloaded from https://agupubs.onlinelibrary.wiley.com/doi/10.1029/2026JG010169 by Florida State University, Wiley Online Library on [02/11/2026]. See the Terms and Conditions (https://onlinelibrary.wiley.com/terms-and-conditions) on Wiley Online Library for rules of use; OA articles are governed by the applicable Creative Commons License

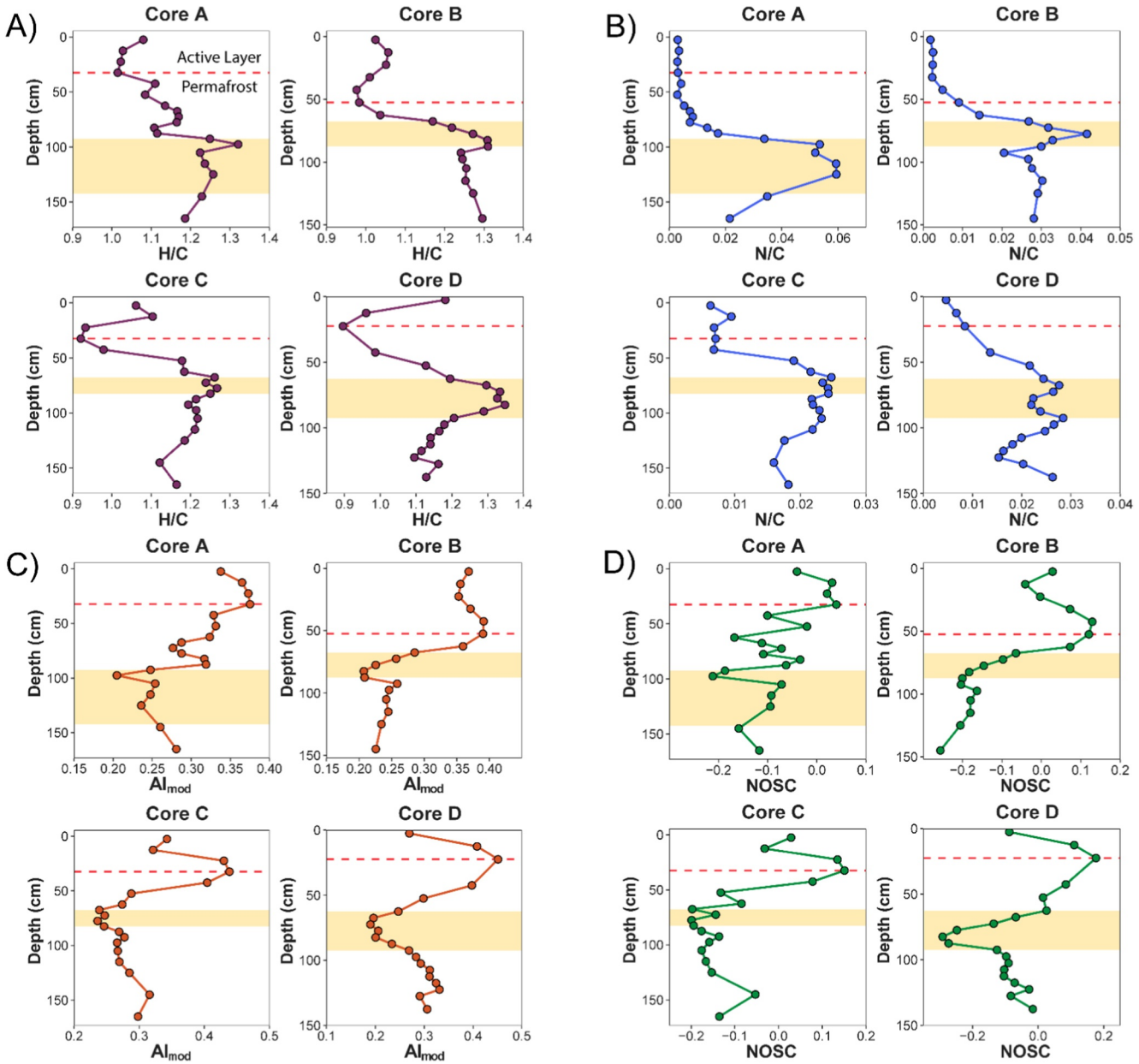


Figure 3. Downcore trends in mean FT-ICR MS derived H/C (a), N/C (b), AI_{mod} (c), and NOSC (d) for A, B, C, and D cores. Red dashed lines indicate maximum annual active layer depth while shaded yellow regions indicate observed zones of DOC enrichment within permafrost peat.

NOSC, with local minima in both values again found to coincide with the observed zones of DOC enrichment within permafrost peat (Figures 3c and 3d; Table 1). While this relative enrichment was more apparent in certain cores, for example, Core D where the distinction between samples of the zone of enrichment and surrounding permafrost was most pronounced, reported elemental ratio, NOSC and AI_{mod} values generally indicated higher proportions of saturated nitrogenous DOM found within the observed zones of DOC enrichment within perennially frozen peat when compared to surrounding permafrost and active layer porewaters (Figures 3 and 4; Table 1).

3.2.2. DOM Compound Class Distributions With Depth

The DOM pool of active layer porewaters was predominantly composed of polyphenolic and highly unsaturated-high O/C compounds (Figure 5; Table 1). Permafrost was generally enriched in aliphatic compounds in

21698961, 2026, 9, Downloaded from https://agupubs.onlinelibrary.wiley.com/doi/10.1029/2026JG010169 by Florida State University, Wiley Online Library on [02/11/2026]. See the Terms and Conditions (https://onlinelibrary.wiley.com/terms-and-conditions) on Wiley Online Library for rules of use; OA articles are governed by the applicable Creative Commons License

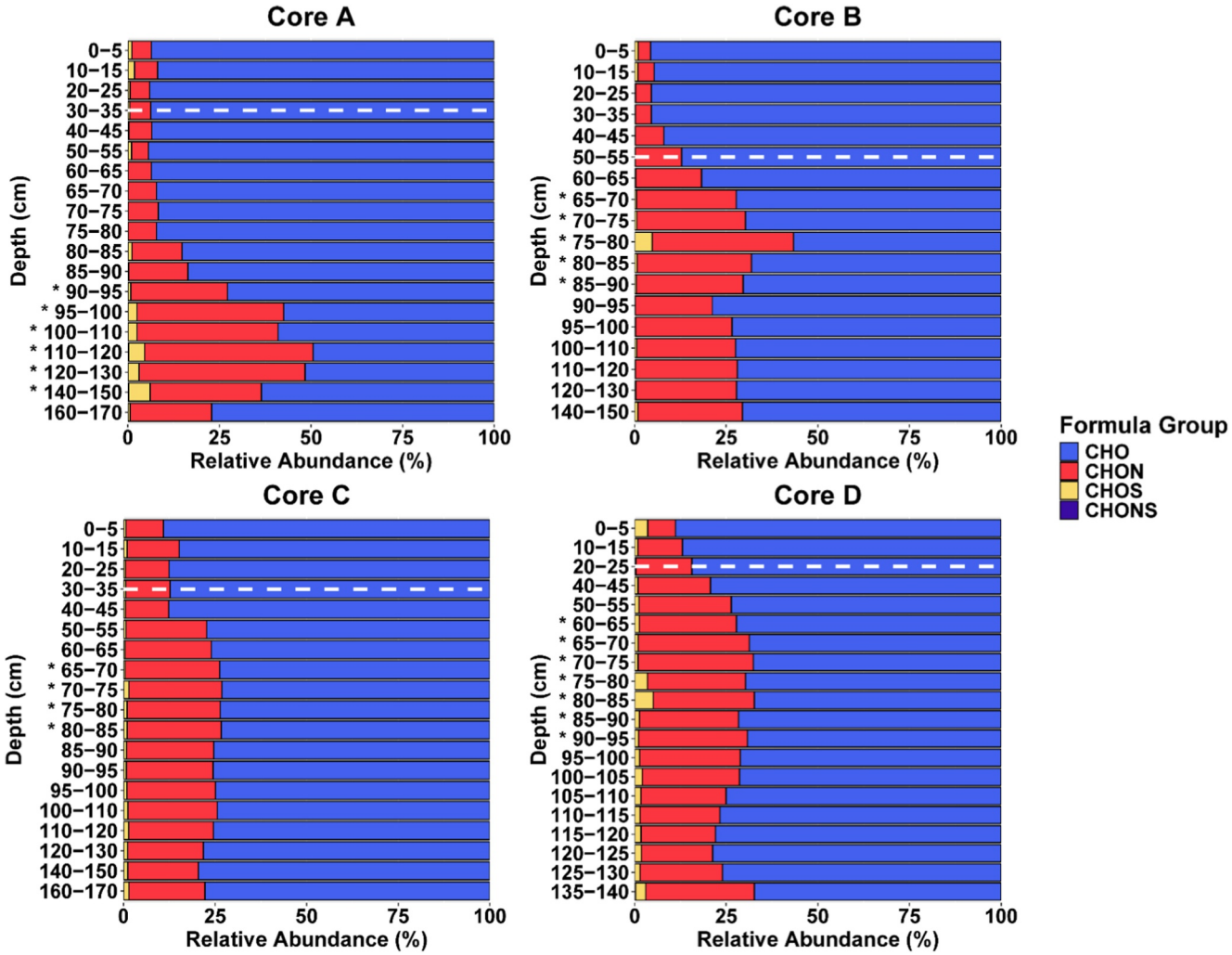


Figure 4. Downcore trends in DOM formula group relative abundance (%) for A, B, C, and D cores. Dashed white lines represent maximum annual active layer depth while asterisks next to particular depth ranges indicate observed zones of DOC enrichment within permafrost peat.

comparison to active layer porewaters (Figure 5; Table 1) ($p < 0.01$), with aliphatic compound relative abundance found to be strongly positively correlated with DOC in samples located within permafrost sections of cores ($\rho = 0.78$, $p = 0$). Downcore trends in compound class relative abundance again demonstrated distinct local "peaks" in the relative abundance of high-energy aliphatic compounds coinciding with the observed zones of DOC enrichment within permafrost peat (Figure 5). Specifically, approximately one-quarter (24.71 ± 5.73%) of the DOM pool in samples corresponding to these zones of DOC enrichment within perennially frozen peat was found to be composed of highly saturated aliphatic compounds, a notable difference when compared to surrounding permafrost layers that demonstrated generally lower DOM aliphaticity (14 ± 5.46%) ($p < 0.01$) (Table 1). Analysis of unique molecular formulae found within active layer porewaters, localized zones of DOC enrichment within permafrost peat, and surrounding permafrost layers further demonstrated strong distinctions in the molecular character of DOM found within each of these depth ranges (Figure 6). Bulk permafrost peat (including zones of enrichment) of these cores contained a suite of nitrogenous aliphatic formulae absent from active layer porewaters (Figure 6b). Comparison of molecular formulae found within samples corresponding to localized zones of DOC enrichment within permafrost versus surrounding permafrost layers highlighted strong heterogeneity in DOM composition with depth in perennially frozen WSL peat, revealing a unique group of molecular formulae found to be present within zones of enrichment but absent from surrounding permafrost layers (Figure 6d). Specifically, a suite of nitrogenous aliphatic formulae unique to localized zones of DOC enrichment within permafrost peat was identified (Figure 6d).

21698961, 2026, 9, Downloaded from https://agupubs.onlinelibrary.wiley.com/doi/10.1029/2026JG010169 by Florida State University, Wiley Online Library on [02/11/2026]. See the Terms and Conditions (https://onlinelibrary.wiley.com/terms-and-conditions) on Wiley Online Library for rules of use; OA articles are governed by the applicable Creative Commons License

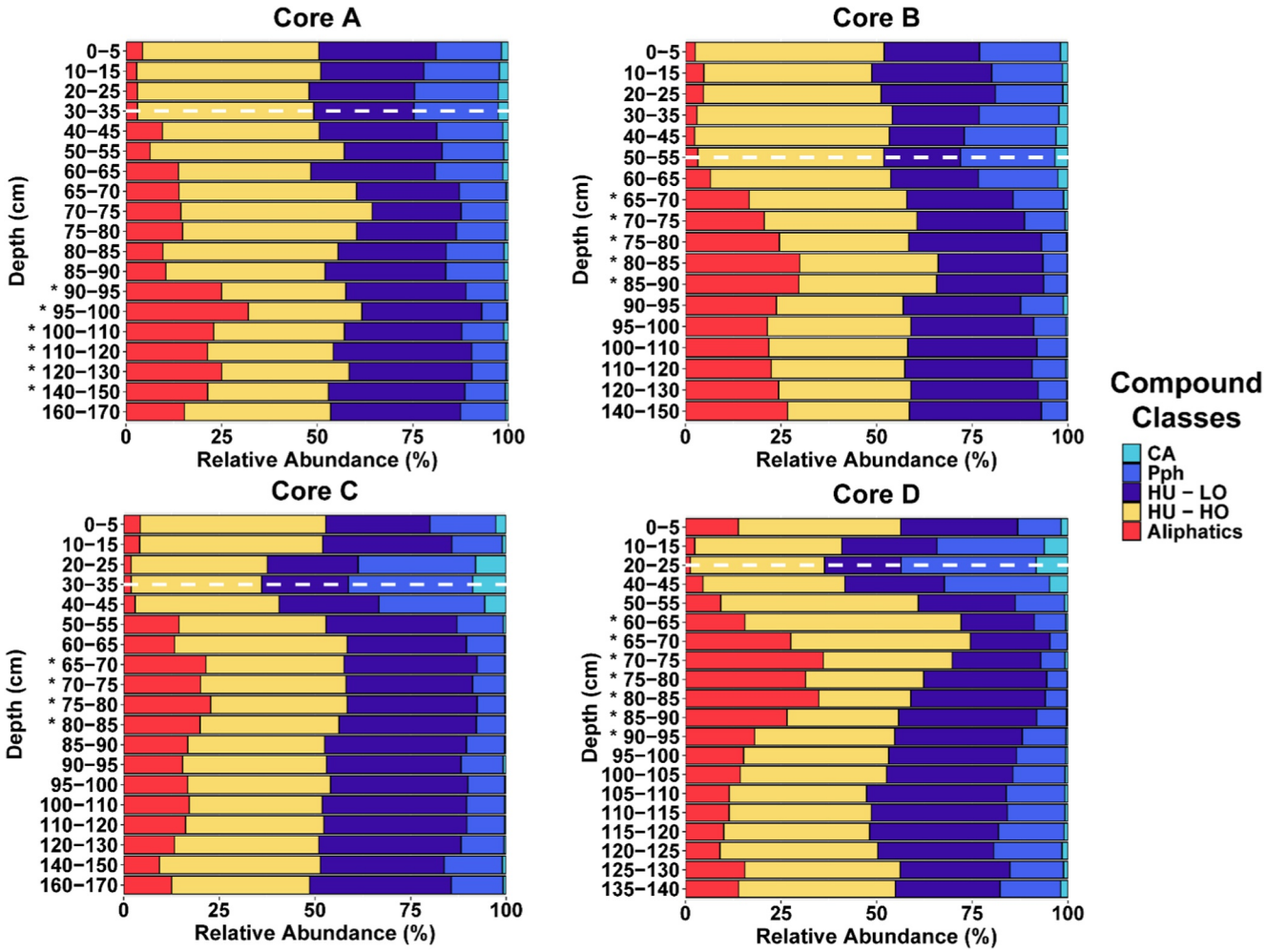


Figure 5. Downcore trends in DOM compound class relative abundance (%) for A, B, C, and D cores. Dashed white lines represent maximum annual active layer depth while asterisks next to depth ranges indicate zones of DOC enrichment within permafrost peat; CA = Condensed Aromatics, Pph = Polyphenolics, HU-LO = Highly Unsaturated–Low O/C, HU-HO = Highly Unsaturated–High O/C.

3.2.3. Multivariate Analysis (PCA)

PCA indicated that component 1 (PC1) and component 2 (PC2) together explained 73.0% of the variance between samples based on DOM molecular properties and DOC concentrations (Figure 7). Strong separation of samples across PC1 (explaining 57.8% of total variance) was apparent, with samples from the active layer strongly related by higher molecular weight and more aromatic DOM character as indicated by their apparent correlation with NOSC, AI_{mod}, polyphenolics, and average mass (Figure 7). Samples from zones of DOC enrichment within permafrost peat, by contrast, demonstrated strong positive correlation to PC1, and were related by high H/C, aliphatic content, N/C and CHON (Figure 7), together reinforcing the observed highly saturated N-enriched character of DOM within these particular permafrost depth ranges. Samples from permafrost layers surrounding zones of enrichment clustered near the origin in PCA space, indicating DOM molecular characteristics intermediate of active layer porewaters and zones of enrichment (Figure 7). Taken together, the PCA demonstrated that separation of samples across PC1 based on DOM molecular composition was more strongly driven by location within the depth profile of WSL permafrost peatlands as opposed to micro-landscape variability (Figure 7), with the greatest degree of compositional dissimilarity observed between highly aromatic active layer DOM pools and zone of enrichment DOM pools, found to be locally enriched in aliphatic compounds when compared to surrounding depth ranges within WSL permafrost peat.

21698961, 2026, 9, Downloaded from https://agupubs.onlinelibrary.wiley.com/doi/10.1029/2026JG010169 by Florida State University, Wiley Online Library on [02/11/2026]. See the Terms and Conditions (https://onlinelibrary.wiley.com/terms-and-conditions) on Wiley Online Library for rules of use; OA articles are governed by the applicable Creative Commons License

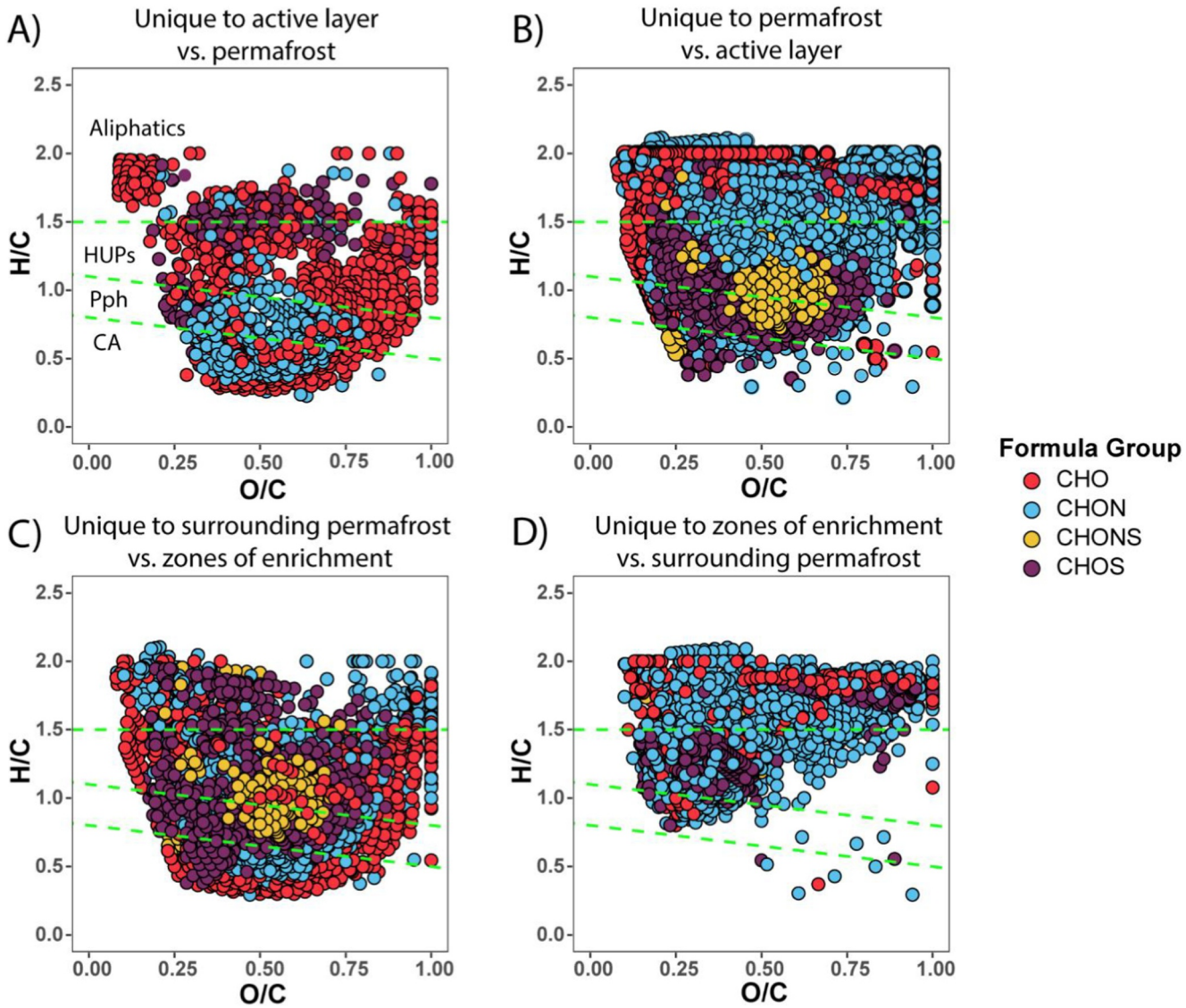


Figure 6. van Krevelen diagrams of molecular formulae unique to distinct peat core regions, where (a) shows formulae unique to active layer peat versus permafrost peat, (b) shows formulae unique to permafrost peat versus active layer peat, (c) shows formulae unique to surrounding permafrost depth ranges versus zones of enrichment and (d) shows formulae unique to zones of enrichment versus surrounding permafrost depth ranges; HUPs = Highly Unsaturated and Phenolic Compounds, Pph = Polyphenolics, and CA = Condensed Aromatics.

4. Discussion

4.1. Patterns of DOM Composition and Potential Reactivity With Depth

The relatively N-enriched, aliphatic character of permafrost DOM versus active layer porewater DOM (Figures 5 and 6; Table 1) observed here corroborates the findings of previous studies documenting the molecular composition of DOM derived from Alaskan and Siberian permafrost deposits (Bristol et al., 2024; Starr et al., 2024). The prevalence of this particular heteroatom-rich, aliphatic formulae group within permafrost as revealed by these FT-ICR MS-based studies has previously been linked to the relatively high biolability of permafrost DOM upon thaw (Bristol et al., 2024; Wickland et al., 2018); with the preferential remineralization of these formulae by microbial communities found to occur in natural systems and biodegradation experiments, presumably due to their high-energy content as well as microbial metabolic N and S demands (Bristol et al., 2024; Drake et al., 2015). Interestingly, OM in permafrost peat from other regions, such as the Western Canadian Arctic, has been shown to be relatively biostable upon thaw as evidenced by molecular-level investigations into the

21698961, 2026, 9, Downloaded from https://agupubs.onlinelibrary.wiley.com/doi/10.1029/2026JG010169 by Florida State University, Wiley Online Library on [02/11/2026]. See the Terms and Conditions (https://onlinelibrary.wiley.com/terms-and-conditions) on Wiley Online Library for rules of use; OA articles are governed by the applicable Creative Commons License

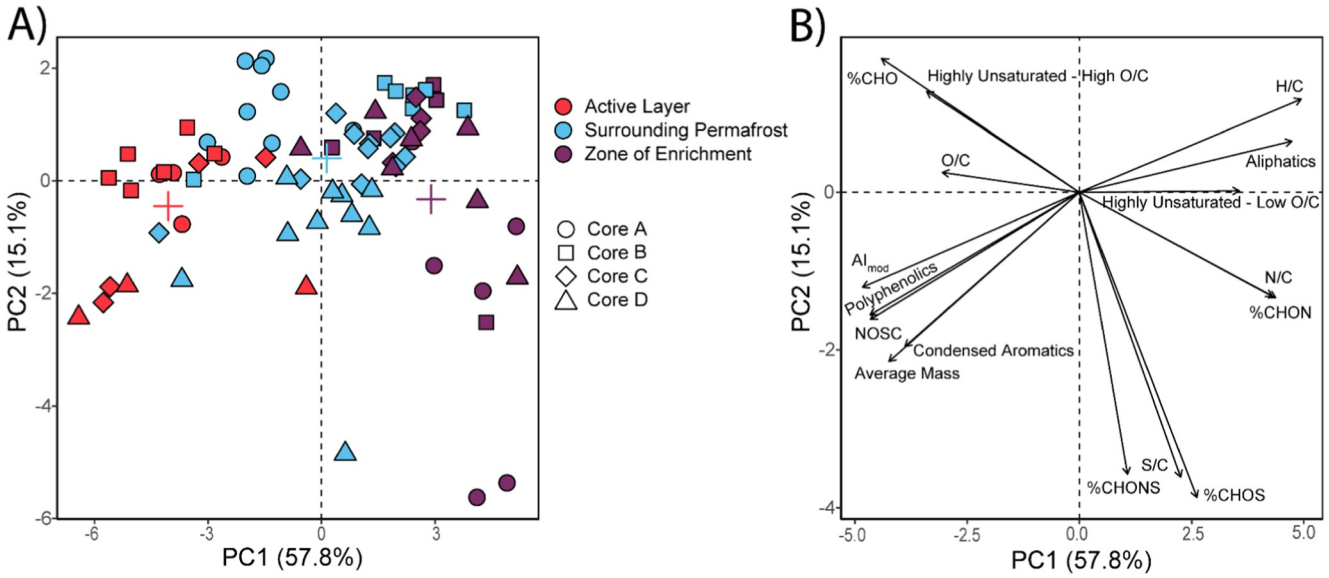


Figure 7. Principal Component Analysis scores (a) and loadings (b) with samples from each core (shape) colored by group within peat core depth profile and group centroids depicted by crosses.

composition of these deposits as well as laboratory biodegradation experiments (Estop-Aragonés et al., 2022; Harris et al., 2023). These conflicting observations may be attributable to: (a) inherent differences existing between examined OM pools of this study (porewater DOM) and of previous studies (bulk peat OM); (b) biases in the pools captured by FT-ICR MS vs. analytical methods of previous studies, or; (c) regional differences in landscape history, with the syngenetic formation of northern WSL permafrost peat potentially resulting in enhanced cryopreservation of biolabile aliphatic compounds when compared to other studied locations where permafrost peat formed epigenetically (Manies et al., 2021).

While relative abundance of aliphatic compounds has typically been found to increase with depth in yedoma-focused studies, demonstrating an apparent correlation between deposit age and potential DOM biolability upon thaw (Heslop et al., 2019; Stapel et al., 2018), here we observe that the highest proportion of potentially biolabile DOM within WSL permafrost peat coincides with the apparent zones of DOC enrichment located between ~70 and 90 cm depth for Cores B, C, and D and ~90 and 150 cm depth for Core A, as indicated by the local peaks in N-containing aliphatic compound relative abundance occurring at these depth ranges (Figures 3, 5, and 6d). This observed relationship between DOC concentration and relative abundance of N-enriched aliphatic compounds within WSL permafrost suggests that the depth-dependent remobilization potential of permafrost DOM in this region and the potential bioavailability of this DOM to local microbial communities may be strongly coupled. This may potentially be supported by the absence of this correlation in active layer porewaters, suggesting aliphatic compound remineralization and/or hydrologic redistribution upon thaw (Pérez-Serrano et al., 2026). The relationship between DOC and DOM aliphaticity within permafrost observed here is also supported by previous studies examining downcore trends in $SUVA_{254}$ (optical absorbance at 254 nm relative to DOC concentration), which have identified similar trends in peat cores collected from the forest tundra and northern taiga biomes of the WSL as well as Tazovsky (Lim et al., 2021), suggesting that this phenomenon may potentially span a broad latitudinal range within the vast WSL permafrost peatland network. Interestingly, prior work examining depth-dependent distributions of biolabile LMWOAs within WSL permafrost peat has also documented trends mirroring the findings of this study, identifying zones of peak carboxylate and DOC concentration consistently occurring between 70 and 100 cm depth within cores taken from the sporadic permafrost zone of the WSL (Kuzmina et al., 2023) as well as the Tazovsky cores examined in this study (Pérez-Serrano et al., 2026). Taken together, this indicates that these particular depth ranges, in addition to their well-documented enrichment in DOC, alkali and alkaline-earth metals, sulfate, phosphorus, and trace metals (Lim et al., 2021; Pérez-Serrano et al., 2026), also represent locally enriched repositories of highly biodegradable permafrost OM pool constituents within perennially frozen WSL peat, namely low-molecular weight, N-enriched aliphatic

21698961, 2026, 9, Downloaded from https://agupubs.onlinelibrary.wiley.com/doi/10.1029/2026JG010169 by Florida State University, Wiley Online Library on [02/11/2026]. See the Terms and Conditions (https://onlinelibrary.wiley.com/terms-and-conditions) on Wiley Online Library for rules of use; OA articles are governed by the applicable Creative Commons License

compounds and LMWOAs. As such, these observed zones of enrichment likely represent potential "biolability hotspots" (McClain et al., 2003) within WSL permafrost depth profiles that have potentially preconditioned non-linear post-thaw GHG production from these peatlands with forecast warming across the WSL region.

In the case of thermokarst and post-thaw formation of shallow lake/pond environments, the higher relative abundance of aliphatic compounds found within the observed zones of enrichment may render a higher proportion of frozen DOM in these depth ranges potentially susceptible to remineralization as CH_4 (Heslop et al., 2019) contingent on post-thaw redox conditions. This, when coupled with the observed local maxima in DOC and methanogenesis-amenable LMWOA concentrations found within these zones of enrichment by other studies (Kuzmina et al., 2023; Lim et al., 2021; Pérez-Serrano et al., 2026), suggests that (from a purely substrate-level perspective) these particular depth ranges may likely contribute to considerably larger pulses (i.e., hot moments) of CH_4 release under thermodynamically favorable conditions versus surrounding permafrost peat layers upon thaw. Given that CH_4 emissions from shallow thermokarst ponds are currently estimated to account for over two-thirds of total CH_4 emissions from regions above 50°N globally (Le Moigne et al., 2020; Wik et al., 2016), this observation suggests that the continued formation of these thaw features that mobilize DOM from zone of enrichment depth ranges across the WSL may have the potential to enhance this globally significant high-latitude CH_4 source in the coming decades.

In addition to potentially driving higher carbonaceous GHG production upon thaw, the substantial enrichment in TN and CHON-containing compounds as well as high DOM N/C ratios observed here within permafrost peat (particularly within zone of enrichment depth ranges) (Figures 3b and 4; Table 1) may have the potential to drive enhanced N_2O production from WSL peatlands, specifically by increasing biolabile organic and inorganic N availability. This phenomenon has previously been suggested for other regions of the permafrost domain, particularly upland environments characterized by ice-rich yedoma deposits containing low C:N ratios (Marushchak et al., 2021; Strauss et al., 2022). While the release of bioavailable organic and inorganic N forms from zone of enrichment depth ranges may (exclusively from a substrate level point of view) be conducive to hot moments of microbial N_2O production, this effect may be potentially less pronounced in WSL peatlands when compared to yedoma uplands given the predominance of waterlogged, acidic bog conditions that promote complete denitrification to N_2 as opposed to N_2O, as well as the potential for high post-thaw vegetative nutrient uptake in these systems (Strauss et al., 2022). Such a fertilization effect on local vegetation communities could potentially offset future permafrost C losses by contributing to enhanced post-thaw surficial peat accumulation, as has previously been documented within thermokarst bogs of Western Canada (Heffernan et al., 2020).

Interactions between WSL permafrost DOM, nutrient elements and microbial communities will ultimately prove crucial in determining post-thaw GHG production from these systems. Studies from the yedoma domain have previously documented the presence of methanogens within both shallow and deep permafrost deposits (Heslop et al., 2019), indicating that these frozen microbial communities are likely readily equipped to metabolize OM as CH_4 following thaw. However, microbiological studies of shallow thermokarst pond environments across the Arctic Siberian tundra have highlighted significant variability in the bacterial community composition of these thaw features, in some cases demonstrating the potential of pelagic methanotrophs to mitigate CH_4 emissions from these water bodies (Le Moigne et al., 2020). The high concentrations of redox-active Fe and Mn present within zone of enrichment depth ranges (Lim et al., 2021; Pérez-Serrano et al., 2026) will also likely prove significant in driving net microbial CH_4 production versus consumption following permafrost thaw. It is well established that Fe and Mn may either enhance or inhibit methanogenesis depending on factors including oxidation state and concentration (Zhuang et al., 2015). Given that metal micronutrients in WSL permafrost have previously been found to reside in predominantly low molecular weight, dissolved forms (Lim et al., 2022; Pérez-Serrano et al., 2026), thaw of zone of enrichment depth ranges may provide essential Fe(II) required for methanogen metalloenzymes (Payne et al., 2021). In any case, it is readily apparent further research is needed to accurately predict the biogeochemical repercussions of WSL permafrost thaw under future climate warming scenarios given that the zones of enrichment documented here are local features, and that the relative magnitude of abrupt versus gradual thaw processes in this region will undoubtedly complicate predictions of solute remobilization (including inorganic N speciation), post-thaw redox conditions, microbial community assemblage, functional diversity, and hence magnitude and speciation of GHG emissions from these systems over the course of this century.

21698961, 2026, 9, Downloaded from https://agupubs.onlinelibrary.wiley.com/doi/10.1029/2026JG010169 by Florida State University, Wiley Online Library on [02/11/2026]. See the Terms and Conditions (https://onlinelibrary.wiley.com/terms-and-conditions) on Wiley Online Library for rules of use; OA articles are governed by the applicable Creative Commons License

4.2. Potential Implications for Aquatic Biogeochemistry of the WSL

In addition to their potential to accelerate GHG production in this region, thawing of the observed zones of enrichment within WSL permafrost may introduce large quantities of aged DOM into local hydrologic networks. It has previously been estimated that a 1 m deepening of the active layer in WSL permafrost peatlands may remobilize approximately 58 ± 38 Tg of DOC into lake and stream systems of this region (Lim et al., 2021), with our observations suggesting that a significant portion of the mobilized DOM may likely consist of highly saturated aliphatic DOC and DON. Earlier studies modeling the impacts of projected climate warming on the WSL suggest that by the end of the current century, rivers of this region will experience a 32%–53% increase in DON concentrations and 30%–50% increase in TDN concentrations (Frey et al., 2007). Our observations demonstrate that thawing permafrost peat of this region may contribute considerably to this projected increase, given the relative enrichment of TN and CHON-containing compounds within perennially frozen versus active layer peat (Figure 4; Table 1). In particular, we suggest that thawing of zone of enrichment depth ranges will drive a nonlinear response (i.e., hot moments) of increases in DON and TDN across the WSL region over the course of this century, given their relative TN and organic N enrichment in comparison to surrounding permafrost layers (Figures 3b and 4; Table 1), in turn leading to pulses of aquatic DON mobilization associated with the degradation of these particular permafrost peat horizons.

The potential fate of DOM mobilized from thawing WSL permafrost will ultimately be governed by its molecular composition, regional hydrologic connectivity, and aquatic biogeochemical constraints/ambient conditions. The high biodegradability of permafrost-derived DOM in aquatic systems is previously well-documented, with reported DOC losses ranging from 30% to 60% in natural systems and laboratory biodegradation experiments using yedoma permafrost (Abbott et al., 2014; Drake et al., 2015; Spencer et al., 2015). Most of this permafrost DOC remineralization occurs rapidly in small headwater thaw streams or within the first 100 hr of biodegradation experiments simulating these environments (Drake et al., 2015; Spencer et al., 2015), with the preferential remineralization of low molecular weight aliphatic compounds consistently observed in these studies. Given our findings, we suggest that the higher relative abundance of nitrogenous aliphatic compounds and higher TN concentrations observed within zone of enrichment depth ranges may result in elevated delivery of DIC, NH_4^+ and NO_3^- to riverine and ultimately coastal systems from thawing WSL peatlands versus surrounding permafrost layers (Table 1). While the vast majority of biolabile permafrost DOC and DON may be remineralized prior to entering river main stems (Spencer et al., 2015), given the proximity and strong hydrologic connectivity of permafrost peatlands in the WSL region to the Kara Sea, it is possible (under conditions when active layers are well-connected with aquatic networks, e.g. during late summer storm events) that a portion of these potentially bioavailable compounds may still be transported relatively unaltered to coastal zones of this region upon thaw. This possibility is supported by a related study that employed a coupled stoichiometric and decay-rate model with respect to the fate of dissolved peat porewater constituents within these cores, which found that large portions of DOC and dissolved N remain available for lateral export as a result of rapid in situ phosphorus consumption during progressive thaw (Pérez-Serrano et al., 2026). As such, increased flux of this aged, biolabile DOM to the Kara Sea will likely prove significant in shaping changes to coastal zone ecosystem metabolism over the course of this century, particularly during the period of peak permafrost degradation occurring during late summer in these systems (Kurek et al., 2025).

The influence of zone of enrichment depth ranges on aquatic ecosystem processes in this region may be especially significant given the potential for interaction between DOM and other solutes mobilized by thaw during hydrologic transport. The elevated levels of Fe, P, Mg, Ca, Mn, and Sr recorded within these zones of enrichment in addition to the N-containing aliphatic compounds documented here may lead to emergent impacts on DOM biodegradability, driven by interactions between these constituents in WSL waterways. Studies examining interactions between DOM and dissolved Fe and P species have found that solute availability and dissolved versus colloidal forms exert strong control over resultant DOM biodegradability (Xiao et al., 2016). While colloidal Fe forms are known to protect labile fractions of DOM from degradation upon complexation, as has recently been documented in Arctic shelf sediments (Faust et al., 2023; Xiao et al., 2016), dissolved Fe-DOM complexes may enhance microbial growth and in turn biodegradation potential when other nutrients such as P are not limiting (Xiao et al., 2016). Such interactions may prove consequential for zone of enrichment DOM fate upon thaw, given the relative enrichment of these depth ranges in dissolved Fe and P forms (Lim et al., 2021, 2022) as well as N-containing aliphatic compounds that may be particularly prone to complexation with reduced Fe species.

21698961, 2026, 9, Downloaded from https://agupubs.onlinelibrary.wiley.com/doi/10.1029/2026JG010169 by Florida State University, Wiley Online Library on [02/11/2026]. See the Terms and Conditions (https://onlinelibrary.wiley.com/terms-and-conditions) on Wiley Online Library for rules of use; OA articles are governed by the applicable Creative Commons License

21698961, 2026, 9, Downloaded from https://agupubs.onlinelibrary.wiley.com/doi/10.1029/2026JG010169 by Florida State University, Wiley Online Library on [02/11/2026]. See the Terms and Conditions (https://onlinelibrary.wiley.com/terms-and-conditions) on Wiley Online Library for rules of use; OA articles are governed by the applicable Creative Commons License

4.3. Zone of Enrichment Formational Mechanisms

While the exact drivers for the distinct downcore patterns of solute distribution observed in WSL permafrost peatlands have not yet been confirmed, previous studies have proposed several plausible hypotheses explaining the presence of the observed "zones of enrichment" within perennially frozen peat of this region (Kuzmina et al., 2023; Lim et al., 2021). It has previously been suggested that these zones may have formed as a result of converging freeze fronts during past cold periods, with solutes excluded from peat porewaters during freezing becoming concentrated at the point where these fronts met (Lim et al., 2021). While this hypothesis effectively accounts for differences in bulk solute concentrations between permafrost horizons, the higher DOM aliphaticity observed within zones of enrichment versus surrounding permafrost layers here points to the occurrence of DOM molecular fractionation processes in addition to bulk solute exclusion mechanisms. Studies examining the effects of freezing on DOM molecular fractionation in aquatic systems have previously found that ice formation results in the preferential exclusion of high molecular weight aromatic compounds from the surrounding brine, leading to the concentration of primarily low molecular weight aliphatic DOM in ice (Pan et al., 2024; Zhou et al., 2023). While additional factors likely need to be considered when examining the effects of freezing on peat porewater DOM composition, this observation suggests that the convergence of freeze fronts leading to the selective exclusion of aromatic DOM from permafrost may not explain the higher relative abundance of low molecular weight, aliphatic DOM within zone of enrichment depth ranges as observed here.

Another plausible hypothesis is that these zones of enrichment may represent localized paleo active layers (Lim et al., 2021) most likely formed during the early-mid Holocene. Previous studies from northwestern Canada documenting differences in the geochemistry of paleo active layers compared to undisturbed permafrost have found that these relict active layers (specifically those formed during past thaw slumping events) generally contain higher solute concentrations when compared to surrounding permafrost and active layer sediments, resulting in vertical patterns of element concentration within glaciogenic permafrost profiles similar to those documented within WSL permafrost peat (Lacelle et al., 2019; Lim et al., 2021). Additionally, relict active layers formed via past thaw slumping during the early Holocene warm interval have been found to contain well-preserved, Holocene-aged biolabile O-alkyl-C groups in addition to biostable Pleistocene-aged aromatic C forms as assessed by IR spectroscopy (Lacelle et al., 2019). This suggests a fresh input of aliphatic compounds through vegetation recolonization of slumped surface organic mats following thaw, which would later be incorporated into permafrost during climate cooling and permafrost re-aggradation (Heffernan et al., 2024; Lacelle et al., 2019; Slentz et al., 2025). While a detailed examination of peat accumulation rates and paleo active layer position within core depth profiles is currently beyond the scope of this work, it is possible that a similar sequence of events may have occurred in WSL permafrost peatlands during the early-mid Holocene, ensuing as follows: (a) abrupt thaw of ice-rich frozen bogs; (b) enhanced leaching of aliphatic compounds and LMWOAs from hydrophilic sphagnum-like vegetation and active microbial communities that recolonized slumped surficial peat mats; (c) the evapo-concentration of solutes within these mats, all of which may have collectively given rise to the distinct hyper-organic, highly aliphatic "zones of enrichment" within permafrost peat observed here following subsequent climate cooling in this region. This hypothesis is possibly supported by the observation of a considerable suite of nitrogenous aliphatic compounds found to be unique to zone of enrichment depth ranges (Figure 6d) possibly indicative of differences in peat development and N-cycling during past periods of permafrost formation (Heffernan et al., 2024; Slentz et al., 2025), with these low molecular weight aliphatic compounds potentially becoming further concentrated within zones of enrichment through past freeze-thaw cycles (Kuzmina et al., 2023; Lim et al., 2022).

5. Conclusions

In this study, we examined trends in DOM molecular composition as related to presumed biolability upon thaw with depth in permafrost peatlands of the WSL using ultrahigh-resolution FT-ICR MS. Our results lend support to previous studies from this region, demonstrating the potentially high biolability of DOM stored within perennially frozen WSL peat as indicated by its high aliphaticity and N-content in comparison to active layer porewater DOM. We document the presence of localized "zones of enrichment" within WSL permafrost peat, characterized by markedly higher DOC concentrations and relative abundance of N-containing aliphatic compounds when compared to surrounding permafrost depth ranges. While previous work focused on Alaskan yedoma suggests that potential PCF magnitude may strengthen either linearly or exponentially (contingent on RCP trajectory) with continual increases in thaw depth (Heslop et al., 2019), the downcore trends observed in this study point to a

different trajectory for WSL permafrost peatlands (Figures 3 and 5; Table 1). Specifically, our findings suggest that, upon thaw, the depth ranges associated with localized zones of DOC enrichment within WSL permafrost peat will likely exert the strongest effects on global climate forcing. As such, we propose that a biogeochemical "hotspot-hot moment" framework (McClain et al., 2003) is potentially more appropriate in assessing future contributions from WSL permafrost peatlands to global PCF strength. For example, with continued thermokarst lake and pond formation across Western Siberia, abrasion of surrounding frozen peat corresponding to zone of enrichment depth ranges within permafrost may create local hotspots of microbial activity within sediment porewaters (Kurashev et al., 2024), leading to potential non-linear trajectories (or hot moments) of CO_2, CH_4 and N_2O release from these systems (Kurashev et al., 2024; Serikova et al., 2019). Additionally, the downcore trends in DOM molecular composition (specifically CHON enrichment) as well as higher TN concentrations observed here within zones of enrichment point to the potential for outsized contributions from these depth ranges to forecast TDN increases in rivers and coastal marine environments of the WSL, mobilizing a potentially substantial pool of highly biolabile DON with implications for aquatic ecosystem metabolism. Taken together, the observations of this study, coupled with the findings of previous studies documenting Fe, P, Mg, Ca, Mn, and Sr enrichment within these depth ranges highlight the potential for emergent biogeochemical impacts following thaw of these zones of enrichment driven by interactions between these constituents. Ultimately, understanding the composition of DOM within these "zones of enrichment" is fundamentally important for our ability to predict its fate upon thaw with ongoing changes to regional climate and hydrologic regimes, with this study highlighting the significance of local depth features in shaping future biogeochemical impacts and PCF strength with continued warming of the permafrost domain.

Conflict of Interest

The authors declare no conflicts of interest relevant to this study.

Availability Statement

The authors declare that all sample FT-ICR MS data files supporting the results of this study are archived in the Open Science Framework (https://osf.io/v89jw/files/osfstorage).

Acknowledgments
RGMS acknowledges support from the National Science Foundation Belmont Forum Award #2124464, and this research was also supported by Belmont Forum Project No. ANR-21-SOIL-0005-01 (VULCAR-FATE). S. Loiko and A. Lim acknowledges the support of the State Assignment of the Ministry of Science and Higher Education of the Russian Federation (project No. FSWM-2024-0006). A portion of this work was performed at the National High Magnetic Field Laboratory ICR User Facility, which is supported by the National Science Foundation Division of Chemistry and Division of Materials Research through DMR-2128556 and the state of Florida.

References

Abbott, B. W., Larouche, J. R., Jones, J. B., Bowden, W. B., & Balser, A. W. (2014). Elevated dissolved organic carbon biodegradability from thawing and collapsing permafrost. *Journal of Geophysical Research: Biogeosciences*, *119*(10), 2049–2063. https://doi.org/10.1002/2014JG002678

Boye, K., Noël, V., Tfaily, M. M., Bone, S. E., Williams, K. H., Bargar, J. R., & Fendorf, S. (2017). Thermodynamically controlled preservation of organic carbon in floodplains. *Nature Geoscience*, *10*(6), 415–419. https://doi.org/10.1038/ngeo2940

Bristol, E. M., Behnke, M. I., Spencer, R. G. M., McKenna, A., Jones, B. M., Bull, D. L., & McClelland, J. W. (2024). Eroding permafrost coastlines release biodegradable dissolved organic carbon to the Arctic Ocean. *Journal of Geophysical Research: Biogeosciences*, *129*(7), e2024JG008233. https://doi.org/10.1029/2024JG008233

Cheng, F., Garzione, C., Li, X., Salzmann, U., Schwarz, F., Haywood, A. M., et al. (2022). Alpine permafrost could account for a quarter of thawed carbon based on Plio-Pleistocene paleoclimate analogue. *Nature Communications*, *13*(1), 1329. https://doi.org/10.1038/s41467-022-29011-2

Dittmar, T., Koch, B., Hertkorn, N., & Kattner, G. (2008). A simple and efficient method for the solid-phase extraction of dissolved organic matter (SPE-DOM) from seawater. *Limnology and Oceanography: Methods*, *6*, 230–235. https://doi.org/10.4319/lom.2008.6.230

Drake, T. W., Guillemette, F., Hemingway, J. D., Chanton, J. P., Podgorski, D. C., Zimov, N. S., & Spencer, R. G. M. (2018). The ephemeral signature of permafrost carbon in an Arctic fluvial network. *Journal of Geophysical Research: Biogeosciences*, *123*(5), 1475–1485. https://doi.org/10.1029/2017JG004311

Drake, T. W., Wickland, K. P., Spencer, R. G. M., McKnight, D. M., & Striegl, R. G. (2015). Ancient low–molecular-weight organic acids in permafrost fuel rapid carbon dioxide production upon thaw. *Proceedings of the National Academy of Sciences*, *112*(45), 13946–13951. https://doi.org/10.1073/pnas.1511705112

Estop-Aragonés, C., Heffernan, L., Knorr, K.-H., & Olefeldt, D. (2022). Limited potential for mineralization of permafrost peatland soil carbon following thermokarst: Evidence from anoxic incubation and priming experiments. *Journal of Geophysical Research: Biogeosciences*, *127*(12), e2022JG006910. https://doi.org/10.1029/2022JG006910

Ewing, S. A., O'Donnell, J. A., Aiken, G. R., Butler, K., Butman, D., Windham-Myers, L., & Kanevskiy, M. Z. (2015). Long-term anoxia and release of ancient, labile carbon upon thaw of Pleistocene permafrost. *Geophysical Research Letters*, *42*(24), 10730–10738. https://doi.org/10.1002/2015GL066296

Faust, J. C., Ascough, P., Hilton, R. G., Stevenson, M. A., Hendry, K. R., & März, C. (2023). New evidence for preservation of contemporary marine organic carbon by iron in Arctic shelf sediments. *Environmental Research Letters*, *18*(1), 014006. https://doi.org/10.1088/1748-9326/aca780

Frey, K. E., McClelland, J. W., Holmes, R. M., & Smith, L. C. (2007). Impacts of climate warming and permafrost thaw on the riverine transport of nitrogen and phosphorus to the Kara Sea. *Journal of Geophysical Research*, *112*(G4), G04S58. https://doi.org/10.1029/2006JG000369

21698961, 2026, 9, Downloaded from https://agupubs.onlinelibrary.wiley.com/doi/10.1029/2026JG010169 by Florida State University, Wiley Online Library on [02/11/2026]. See the Terms and Conditions (https://onlinelibrary.wiley.com/terms-and-conditions) on Wiley Online Library for rules of use; OA articles are governed by the applicable Creative Commons License

Frey, K. E., & Smith, L. C. (2005). Amplified carbon release from vast West Siberian peatlands by 2100. *Geophysical Research Letters*, *32*(9), L0940. https://doi.org/10.1029/2004GL022025

Harris, L. I., Olefeldt, D., Pelletier, N., Blodau, C., Knorr, K.-H., Talbot, J., et al. (2023). Permafrost thaw causes large carbon loss in boreal peatlands while changes to peat quality are limited. *Global Change Biology*, *29*(19), 5720–5735. https://doi.org/10.1111/gcb.16894

Heffernan, L., Estop-Aragonés, C., Knorr, K. H., & Olefeldt, D. (2024). Changing climatic controls on the greenhouse gas balance of thermokarst bogs during succession after permafrost thaw. *Global Change Biology*, *30*(7), e17388. https://doi.org/10.1111/gcb.17388

Heffernan, L., Estop-Aragonés, C., Knorr, K.-H., Talbot, J., & Olefeldt, D. (2020). Long-term impacts of permafrost thaw on carbon storage in peatlands: Deep losses offset by surficial accumulation. *Journal of Geophysical Research: Biogeosciences*, *125*(3), e2019JG005501. https://doi.org/10.1029/2019JG005501

Heslop, J. K., Winkel, M., Walter Anthony, K. M., Spencer, R. G. M., Podgorski, D. C., Zito, P., et al. (2019). Increasing organic carbon biolability with depth in yedoma permafrost: Ramifications for future climate change. *Journal of Geophysical Research: Biogeosciences*, *124*(7), 2021–2038. https://doi.org/10.1029/2018JG004712

Hugelius, G., Loisel, J., Chadburn, S., Jackson, R. B., Jones, M., MacDonald, G., et al. (2020). Large stocks of peatland carbon and nitrogen are vulnerable to permafrost thaw. *Proceedings of the National Academy of Sciences*, *117*(34), 20438–20446. https://doi.org/10.1073/pnas.1916387117

Kaiser, N. K., Quinn, J. P., Blakney, G. T., Hendrickson, C. L., & Marshall, A. G. (2011). A novel 9.4 Tesla FT-ICR mass spectrometer with improved sensitivity, mass resolution, and mass range. *Journal of the American Society for Mass Spectrometry*, *22*(8), 1343–1351. https://doi.org/10.1007/s13361-011-0141-9

Kellerman, A. M., Dittmar, T., Kothawala, D. N., & Tranvik, L. J. (2019). Persistence of dissolved organic matter in lakes related to its molecular characteristics. *Nature Geoscience*, *12*, 430–435. https://doi.org/10.1038/s41561-019-0340-0

Koch, B. P., & Dittmar, T. (2006). From mass to structure: An aromaticity index for high-resolution mass data of natural organic matter. *Rapid Communications in Mass Spectrometry*, *19*(7), 926–932. https://doi.org/10.1002/rcm.1820

Kurashev, D. G., Manasypov, R. M., Raudina, T. V., Krickov, I. V., Lim, A. G., & Pokrovsky, O. S. (2024). Dissolved organic matter quality in thermokarst lake water and sediments across a permafrost gradient, Western Siberia. *Environmental Research*, *252*, 119115. https://doi.org/10.1016/j.envres.2024.119115

Kurek, M. R., McKenna, A. M., Spencer, R. G. M., Bianchi, T. S., Strickland, M., Medeiros, P. M., & Freeman, K. H. (2020). Deciphering dissolved organic matter: Ionization, dopant, and fragmentation insights via Fourier transform ion cyclotron resonance mass spectrometry. *Environmental Science and Technology*, *54*(24), 16249–16259. https://doi.org/10.1021/acs.est.0c05206

Kurek, M. R., Pokrovsky, O. S., Krickov, I. V., Lim, A. G., Korets, M. A., & Spencer, R. G. M. (2025). Assessing the molecular-level controls of dissolved organic matter cycling in West Siberian Lowland rivers. *Journal of Geophysical Research: Biogeosciences*, *130*(4), e2024JG008537. https://doi.org/10.1029/2024JG008537

Kuzmina, D. M., Lim, A. G., Loiko, S. V., Shefer, N., Shirokova, L. S., Julien, F., et al. (2023). Dispersed ice of permafrost peatlands represents an important source of labile carboxylic acids, nutrients and metals. *Geoderma*, *429*, 116256. https://doi.org/10.1016/j.geoderma.2022.116256

Lacelle, D., Fontaine, M., Pellerin, A., Kokelj, S. V., & Clark, I. D. (2019). Legacy of Holocene landscape changes on soil biogeochemistry: A perspective from paleo-active layers in northwestern Canada. *Journal of Geophysical Research: Biogeosciences*, *124*(9), 2662–2679. https://doi.org/10.1029/2018JG004916

Lê, S., Josse, J., & Husson, F. (2008). FactoMineR: An R package for multivariate analysis. *Journal of Statistical Software*, *25*(1), 1–18. https://doi.org/10.18637/jss.v025.i01

Le Moigne, A., Bartosiewicz, M., Schaepman-Strub, G., Abiven, S., & Pernthaler, J. (2020). The biogeochemical variability of Arctic thermokarst ponds is reflected by stochastic and niche-driven microbial community assembly processes. *Environmental Microbiology*, *11*, 4847–4862. https://doi.org/10.1111/1462-2920.15260

Lim, A. G., Loiko, S., Kuzmina, D., Krickov, I. V., Shirokova, L. S., Kulizhskiy, S., & Pokrovsky, O. S. (2022). Organic carbon and major and trace elements reside in labile low-molecular form in the ground ice of permafrost peatlands. *Environmental Science: Processes and Impacts*, *24*(9), 1443–1459. https://doi.org/10.1039/D1EM00547B

Lim, A. G., Manasypov, R. M., Raudina, T. V., Krickov, I. V., Shirokova, L. S., & Pokrovsky, O. S. (2021). Dispersed ground ice of permafrost peatlands: Potential unaccounted carbon, nutrient and metal sources. *Chemical Geology*, *598*, 120813. https://doi.org/10.1016/j.chemgeo.2022.120813

Loiko, S., Raudina, T., Lim, A., Kuzmina, D., Kulizhskiy, S., & Pokrovsky, O. (2019). Microtopography controls of carbon and related elements distribution in the West Siberian frozen bogs. *Geosciences*, *9*(7), 291. https://doi.org/10.3390/geosciences9070291

MacDonald, E. N., Tank, S. E., Kokelj, S. V., Froese, D. G., & Hutchins, R. H. S. (2021). Permafrost-derived dissolved organic matter composition varies across permafrost end-members in the western Canadian Arctic. *Environmental Research Letters*, *16*(2), 024036. https://doi.org/10.1088/1748-9326/abd971

Manies, K. L., Jones, M. C., Waldrop, M. P., Leewis, M.-C., Fuller, C., Cornman, R. S., & Hoefke, K. (2021). Influence of permafrost type and site history on losses of permafrost carbon after thaw. *Journal of Geophysical Research: Biogeosciences*, *126*(11), e2021JG006396. https://doi.org/10.1029/2021JG006396

Mann, H. B., & Whitney, D. R. (1947). On a Test of whether one of two random variables is stochastically larger than the other. *The Annals of Mathematical Statistics*, *18*(1), 50–60. https://doi.org/10.1214/aoms/1177730491

Marushchak, M. E., Kerttula, J., Diáková, K., Schneider von Deimling, T., Zimov, N., Zimov, S. A., et al. (2021). Thawing Yedoma permafrost is a neglected nitrous oxide source. *Nature Communications*, *12*(1), 7107. https://doi.org/10.1038/s41467-021-27386-2

McClain, M. E., Boyer, E. W., Dent, C. L., Gergel, S. E., Grimm, N. B., Groffman, P. M., et al. (2003). Biogeochemical hot spots and hot moments at the interface of terrestrial and aquatic ecosystems. *Ecosystems*, *6*(4), 301–312. https://doi.org/10.1007/s10021-003-0161-9

Miner, K. R., Turetsky, M. R., Malina, E., Bartsch, A., Treat, C. C., Jorgenson, M. T., et al. (2022). Permafrost carbon emissions in a changing Arctic. *Nature Reviews Earth and Environment*, *3*(1), 55–67. https://doi.org/10.1038/s43017-021-00230-3

Olefeldt, D., Goswami, S., Grosse, G., Hayes, D. J., Hugelius, G., Kuhry, P., et al. (2016). Circumpolar distribution and carbon storage of thermokarst landscapes. *Nature Communications*, *7*(1), 13043. https://doi.org/10.1038/ncomms13043

Pan, T., Zhang, Y., Yang, F., Liao, H., Feng, W., Sun, F., et al. (2024). Characteristics of the presence and migration patterns of DOM between ice and water in the cold and arid Daihai Lake. *Journal of Hydrology*, *637*, 131515. https://doi.org/10.1016/j.jhydrol.2024.131515

Pastukhov, A. V., Marchenko-Vagapova, T., Loiko, S., & Kaverin, D. (2021). Vulnerability of the ancient peat plateaus in Western Siberia. *Plants*, *10*(12), 2813. https://doi.org/10.3390/plants10122813

Payne, D. D., Shepard, E. M., Spietz, R. L., Steward, K. M., Brumfield, S., Young, M., et al. (2021). Examining pathways of iron and sulfur acquisition, trafficking, deployment, and storage in mineral-grown methanogen cells. *Journal of Bacteriology*, *203*(19). https://doi.org/10.1128/jb.00146-21

21698961, 2026, 9, Downloaded from https://agupubs.onlinelibrary.wiley.com/doi/10.1029/2026JG010169 by Florida State University, Wiley Online Library on [02/11/2026]. See the Terms and Conditions (https://onlinelibrary.wiley.com/terms-and-conditions) on Wiley Online Library for rules of use; OA articles are governed by the applicable Creative Commons License

Pérez-Serrano, L., Loiko, S. V., Lim, A., Gandois, L., Hatté, C., Rols, J.-L., & Pokrovsky, O. S. (2026). Cryogenic fractionation and thaw-gradient reorganization of carbon, nutrient and trace element pools in permafrost peatlands [Preprint]. *EGUsphere*. https://doi.org/10.5194/egusphere-2026-3058

Rantanen, M., Karpechko, A. Y., Lipponen, A., Nordling, K., Hyvärinen, O., Ruosteenoja, K., et al. (2022). The Arctic has warmed nearly four times faster than the globe since 1979. *Communications Earth and Environment*, *3*(1), 168. https://doi.org/10.1038/s43247-022-00498-3

Raudina, T. V., Loiko, S. V., Lim, A. G., Manasypov, R. M., Shirokova, L. S., Istigechev, G. I., et al. (2018). Permafrost thaw and climate warming may decrease the CO_2, carbon, and metal concentration in peat soil waters of the Western Siberia Lowland. *Science of the Total Environment*, *634*, 1007–1023. https://doi.org/10.1016/j.scitotenv.2018.04.003

Raudina, T. V., & Loiko, S. V. (2019). Properties and major element concentrations in peat profiles of the polygonal frozen bog in Western Siberia. *IOP Conference Series: Earth and Environmental Science*, *400*(1), 012009. https://doi.org/10.1088/1755-1315/400/1/012009

R Core Team. (2021). *R: A language and environment for statistical computing*. R Foundation for Statistical Computing. Retrieved from https://www.R-project.org/

Šantl-Temkiv, T., Finster, K., Dittmar, T., Hansen, B. M., Thyrhaug, R., Nielsen, N. W., & Karlson, U. G. (2013). Hailstones: A window into the microbial and chemical inventory of a storm cloud. *PLoS One*, *8*(1), e53550. https://doi.org/10.1371/journal.pone.0053550

Savory, J. J., Kaiser, N. K., McKenna, A. M., Xian, F., Blakney, G. T., Rodgers, R. P., et al. (2011). Parts-Per-Billion fourier transform ion Cyclotron resonance Mass measurement accuracy with a "Walking" calibration equation. *Analytical Chemistry*, *83*(5), 1732–1736. https://doi.org/10.1021/ac102943z

Serikova, S., Pokrovsky, O. S., Laudon, H., Krickov, I. V., Lim, A., Manasypov, R. M., & Karlsson, J. (2019). High carbon emissions from thermokarst lakes of Western Siberia. *Nature Communications*, *10*(1), 1552. https://doi.org/10.1038/s41467-019-09592-1

Serreze, M. C., Bromwich, D. H., Clark, M. P., Etringer, A. J., Zhang, T., & Lammers, R. (2002). Large-scale hydro-climatology of the terrestrial Arctic drainage system. *Journal of Geophysical Research*, *108*(D2), 8160. https://doi.org/10.1029/2001JD000919

Shapiro, S. S., & Wilk, M. B. (1965). An analysis of variance test for normality (complete samples). *Biometrika*, *52*(3–4), 591–611. https://doi.org/10.1093/biomet/52.3-4.591

Slentz, A. E., McKenna, A. M., Kellerman, A. M., Holt, A. D., Burns, A. J., Miller, M. G., et al. (2025). Signatures of Arctic change: Molecular-level composition and bioavailability of shifting dissolved organic matter sources. *Journal of Geophysical Research: Biogeosciences*, *130*(7), e2025JG008899. https://doi.org/10.1029/2025JG008899

Smith, D. F., Podgorski, D. C., Rodgers, R. P., Blakney, G. T., & Hendrickson, C. L. (2018). 21 Tesla FT-ICR mass spectrometer for ultrahigh-resolution analysis of complex organic mixtures. *Analytical Chemistry*, *90*(3), 2041–2047. https://doi.org/10.1021/acs.analchem.7b04159

Spencer, R. G. M., Mann, P. J., Dittmar, T., Eglinton, T. I., McIntyre, C., Holmes, R. M., et al. (2015). Detecting the signature of permafrost thaw in Arctic rivers. *Geophysical Research Letters*, *42*(8), 2830–2835. https://doi.org/10.1002/2015GL063498

Stapel, J., Schirrmeister, L., Wetterich, S., Borchers, A., Davydov, S. P., & Fritz, M. (2018). Substrate potential of last interglacial to Holocene permafrost organic matter for future microbial greenhouse gas production. *Biogeosciences*, *14*, 2647–2664. https://doi.org/10.5194/bg-14-2647-2017

Starr, S. F., Frey, K. E., Smith, L. C., Kellerman, A. M., McKenna, A. M., & Spencer, R. G. M. (2024). Peatlands versus permafrost: Landscape features as drivers of dissolved organic matter composition in West Siberian rivers. *Journal of Geophysical Research: Biogeosciences*, *129*(2), e2023JG007797. https://doi.org/10.1029/2023JG007797

Stenson, A. C., Marshall, A. G., & Cooper, W. T. (2003). Exact masses and chemical formulas of individual Suwannee River fulvic acids from ultrahigh resolution electrospray ionization Fourier transform ion cyclotron resonance mass spectra. *Analytical Chemistry*, *75*(6), 1275–1284. https://doi.org/10.1021/ac026106p

Strauss, J., Biasi, C., Sanders, T., Krüger, J. P., Bolshiyanov, D. Y., Günther, F., et al. (2022). A globally relevant stock of soil nitrogen in the Yedoma permafrost domain. *Nature Communications*, *13*(1), 6074. https://doi.org/10.1038/s41467-022-33794-9

Strauss, J., Schirrmeister, L., Grosse, G., Wetterich, S., Ulrich, M., Herzschuh, U., & Hubberten, H.-W. (2013). The deep permafrost carbon pool of the Yedoma region in Siberia and Alaska. *Geophysical Research Letters*, *40*(23), 6165–6170. https://doi.org/10.1002/2013GL058088

Tarnocai, C., Canadell, J. G., Schuur, E. A. G., Kuhry, P., Mazhitova, G., & Zimov, S. (2009). Soil organic carbon pools in the northern circumpolar permafrost region. *Global Biogeochemical Cycles*, *23*(2), GB2023. https://doi.org/10.1029/2008GB003327

Textor, S. R., Guillemette, F., Zito, P. A., & Spencer, R. G. M. (2018). An assessment of dissolved organic carbon biodegradability and priming in blackwater systems. *Journal of Geophysical Research: Biogeosciences*, *123*(9), 2998–3015. https://doi.org/10.1029/2018JG004470

Turetsky, M. R., Abbott, B. W., Jones, M. C., Schuur, E. A. G., Grosse, G., Koven, C., et al. (2020). Carbon release through abrupt permafrost thaw. *Nature Geoscience*, *13*(2), 138–143. https://doi.org/10.1038/s41561-019-0526-0

Walter Anthony, K. M., Daanen, R. P., Anthony, P., Schneider von Deimling, T., Ping, C. L., Chanton, J. P., et al. (2016). Methane emissions proportional to permafrost carbon thawed. *Nature*, *538*, 235–239. https://doi.org/10.1038/nature19744

Walvoord, M. A., & Striegl, R. G. (2007). Increased groundwater to stream discharge from permafrost thawing. *Geophysical Research Letters*, *34*, L12402. https://doi.org/10.1029/2007GL030216

Wickham, H. (2016). Programming with ggplot2. In *Ggplot2: Elegant graphics for data analysis* (pp. 241–253). Springer International Publishing.

Wickland, K. P., Waldrop, M. P., Aiken, G. R., Koch, J. C., Jorgenson, M. T., & Striegl, R. G. (2018). Dissolved organic carbon and nitrogen release from boreal Holocene permafrost and seasonally frozen soils of Alaska. *Environmental Research Letters*, *13*(6), 065011. https://doi.org/10.1088/1748-9326/aac4ad

Wik, M., Varner, R. K., Anthony, K. M. W., MacIntyre, S., Bastviken, D., & Karlsson, J. (2016). Climate-sensitive northern lakes and ponds are critical components of methane release. *Nature Geoscience*, *9*(2), 99–105. https://doi.org/10.1038/ngeo2578

Wild, B., Shakhova, N., Dudarev, O. V., Semiletov, I. P., Gustafsson, Ö., others, et al. (2022). Organic matter composition and greenhouse gas production of thawing subsea permafrost in the Laptev Sea. *Nature Communications*, *13*(1), 5057. https://doi.org/10.1038/s41467-022-32696-0

Xiao, Y. H., Hoikkala, L., Kasurinen, V., Tiirola, M., Kortelainen, P., & Vähätalo, A. V. (2016). The effect of iron on the biodegradation of natural dissolved organic matter. *Journal of Geophysical Research: Biogeosciences*, *121*(10), 2544–2561. https://doi.org/10.1002/2016JG003394

Zhou, Y., Hiller, C., Andersson, S., Jakobsson, E., Zhou, L., Hawkes, J. A., et al. (2023). Selective exclusion of aromatic organic carbon during lake ice formation. *Geophysical Research Letters*, *50*(4), e2022GL101414. https://doi.org/10.1029/2022GL101414

Zhuang, L., Xu, J., Tang, J., & Zhou, S. (2015). Effect of ferrihydrite biomineralization on methanogenesis in an anaerobic incubation from paddy soil. *Journal of Geophysical Research: Biogeosciences*, *120*(5), 876–886. https://doi.org/10.1002/2014JG002893

21698961, 2026, 9, Downloaded from https://agupubs.onlinelibrary.wiley.com/doi/10.1029/2026JG010169 by Florida State University, Wiley Online Library on [02/11/2026]. See the Terms and Conditions (https://onlinelibrary.wiley.com/terms-and-conditions) on Wiley Online Library for rules of use; OA articles are governed by the applicable Creative Commons License